

therefore represent promising directions for future study.

Conclusion. Given the ever-growing, technology-driven data stream in today's scientific world, there is an increasing need for tools to make sense of complex data sets in diverse fields. The ability to examine all potentially interesting relationships in a data set—independent of their form—allows tremendous versatility in the search for meaningful insights. On the basis of our tests, MINE is useful for identifying and characterizing structure in data.

References and Notes

1. T. Hastie, R. Tibshirani, J. H. Friedman, *The Elements of Statistical Learning: Data Mining, Inference, and Prediction* (Springer Verlag, New York, 2009).
2. Science Staff, *Science* **331**, 692 (2011).
3. By "functional relationship" we mean a distribution (X, Y) in which Y is a function of X , potentially with independent noise added.
4. A. Caspi *et al.*, *Science* **301**, 386 (2003).
5. R. N. Clayton, T. K. Mayeda, *Geochim. Cosmochim. Acta* **60**, 1999 (1996).
6. T. J. Algeo, T. W. Lyons, *Paleoceanography* **21**, PA1016 (2006).
7. World Health Organization Statistical Information Systems, *World Health Organization Statistical Information Systems (WHOSIS)* (2009); www.who.int/whosis/en/.
8. A. Rényi, *Acta Math. Hung.* **10**, 441 (1959).
9. C. J. Stone, *Ann. Stat.* **5**, 595 (1977).
10. W. S. Cleveland, S. J. Devlin, *J. Am. Stat. Assoc.* **83**, 596 (1988).
11. For both splines and regression estimators, we used R^2 with respect to the estimated spline/regression function to score relationships.
12. Y. I. Moon, B. Rajagopalan, U. Lall, *Phys. Rev. E Stat. Phys. Plasmas Fluids Relat. Interdiscip. Topics* **52**, 2318 (1995).
13. G. Darbellay, I. Vajda, *IEEE Trans. Inf. Theory* **45**, 1315 (1999).
14. A. Kraskov, H. Stögbauer, P. Grassberger, *Phys. Rev. E Stat. Nonlin. Soft Matter Phys.* **69**, 066138 (2004).
15. L. Breiman, J. H. Friedman, *J. Am. Stat. Assoc.* **80**, 580 (1985).
16. T. Hastie, W. Stuetzle, *J. Am. Stat. Assoc.* **84**, 502 (1989).
17. R. Tibshirani, *Stat. Comput.* **2**, 183 (1992).
18. B. Kégl, A. Krzyzak, T. Linder, K. Zeger, *Adv. Neural Inf. Process. Syst.* **11**, 501 (1999).
19. P. Delicado, M. Smrekar, *Stat. Comput.* **19**, 255 (2009).
20. "Principal curve-based methods" refers to mean-squared error relative to the principal curve, and CorGC, the principal curve-based measure of dependence of Delicado *et al.*
21. G. Székely, M. Rizzo, *Ann. Appl. Stat.* **3**, 1236 (2009).
22. B. P. Tu, A. Kudlicki, M. Rowicka, S. L. McKnight, *Science* **310**, 1152 (2005).
23. R. Fisher, Tests of significance in harmonic analysis. *Proc. R. Soc. Lond. A* **125**, 54 (1929).
24. M. Ahdesmäki, H. Lähdesmäki, R. Pearson, H. Huttunen, O. Yli-Harja, *BMC Bioinformatics* **6**, 117 (2005).
25. H. Rosling, Gapminder, *Indicators in Gapminder World* (2008); www.gapminder.org/data/
26. P. T. Spellman *et al.*, *Mol. Biol. Cell* **9**, 3273 (1998).
27. Baseball Prospectus Statistics Reports (2009); www.baseballprospectus.com/sortable/
28. S. Lahman, The Baseball Archive, *The Baseball Archive* (2009); baseball1.com/statistics/
29. P. J. Turnbaugh *et al.*, The effect of diet on the human gut microbiome: A metagenomic analysis in humanized gnotobiotic mice. *Sci. Transl. Med.* **1**, 6ra14 (2009).
30. L. Chen *et al.*, *Lancet* **364**, 1984 (2004).
31. S. Desai, S. Alva, *Demography* **35**, 71 (1998).
32. S. Gupta, M. Verhoeven, *J. Policy Model.* **23**, 433 (2001).
33. T. Gill *et al.*, Obesity in the Pacific: Too big to ignore. *Noumea, New Caledonia: World Health Organization Regional Office for the Western Pacific, Secretariat of the Pacific Community* (2002).
34. RPLMV estimates how many more runs per game a player contributes over a replacement-level player in an average lineup.
35. P. J. Turnbaugh *et al.*, *Nature* **449**, 804 (2007).
36. R. E. Ley *et al.*, *Science* **320**, 1647 (2008).
37. *The World Factbook 2009* (Central Intelligence Agency, Washington, DC, 2009).

Acknowledgments: We thank C. Blättler, B. Eidelson, M. D. Finucane, M. M. Finucane, M. Fujihara, T. Gingrich, E. Goldstein, R. Gupta, R. Hahne, T. Jaakkola, N. Laird, M. Lipsitch, S. Manber, G. Nicholls, A. Papageorge, N. Patterson, E. Phelan, J. Rinn, B. Ripley, I. Shylakhter, and R. Tibshirani for invaluable support and critical discussions throughout; and O. Derby, M. Fitzgerald, S. Hart, M. Huang, E. Karlsson, S. Schaffner, C. Edwards, and D. Yamins for assistance. P.C.S. and this work are supported by the Packard Foundation. For data set analysis, P.C.S. was also supported by NIH MIDAS award U54GM088558, D.N.R. by a Marshall Scholarship, M.M. by NSF grant 0915922, H.K.F. by ERC grant 239985, S.R.G. by the Medical Scientist Training Program, and P.J.T. by NIH P50 GM068763. Data and software are available online at <http://exploredata.net>.

Supporting Online Material

www.sciencemag.org/cgi/content/full/334/6062/1518/DC1
Materials and Methods
SOM Text
Figs. S1 to S13
Tables S1 to S14
References (38–54)

10 March 2011; accepted 5 October 2011
10.1126/science.1205438

The Structure of the Eukaryotic Ribosome at 3.0 Å Resolution

Adam Ben-Shem,*† Nicolas Garreau de Loubresse,* Sergey Melnikov,* Lasse Jenner, Gulnara Yusupova, Marat Yusupov†

Ribosomes translate genetic information encoded by messenger RNA into proteins. Many aspects of translation and its regulation are specific to eukaryotes, whose ribosomes are much larger and intricate than their bacterial counterparts. We report the crystal structure of the 80S ribosome from the yeast *Saccharomyces cerevisiae*—including nearly all ribosomal RNA bases and protein side chains as well as an additional protein, Stm1—at a resolution of 3.0 angstroms. This atomic model reveals the architecture of eukaryote-specific elements and their interaction with the universally conserved core, and describes all eukaryote-specific bridges between the two ribosomal subunits. It forms the structural framework for the design and analysis of experiments that explore the eukaryotic translation apparatus and the evolutionary forces that shaped it.

Ribosomes are responsible for the synthesis of proteins across all kingdoms of life. The core, which is universally conserved and was described in detail by structures of prokaryotic ribosomes, catalyzes peptide bond formation and decodes mRNA (1). However, eukaryotes and prokaryotes differ markedly in other translation processes such as initiation, termination, and regulation (2, 3), and eukaryotic ribosomes play a central role in many eukaryote-

specific cellular processes. Accordingly, eukaryotic ribosomes are at least 40% larger than their bacterial counterparts as a result of additional ribosomal RNA (rRNA) elements called expansion segments (ESs) and extra protein moieties (4).

All ribosomes are composed of two subunits. The large 60S subunit of the eukaryotic ribosome (50S in bacteria) consists of three rRNA molecules (25S, 5.8S, and 5S) and 46 proteins, whereas the small 40S subunit (30S in bacteria)

includes one rRNA chain (18S) and 33 proteins. Of the 79 proteins, 32 have no homologs in crystal structures of bacterial or archaeal ribosomes, and those that do have homologs can still harbor large eukaryote-specific extensions (5). Apart from variability in certain rRNA expansion segments, all eukaryotic ribosomes, from yeast to human, are very similar.

Three-dimensional cryoelectron microscopy (cryo-EM) reconstructions of eukaryotic ribosomes at 15 to 5.5 Å resolution provided insight into the interactions of the ribosome with several factors (4, 6–8). A crystal structure of the *S. cerevisiae* ribosome at 4.15 Å resolution described the fold of all ordered rRNA expansion segments, but the relatively low resolution precluded localization of most eukaryote-specific proteins (9). Crystallographic data at a better resolution (3.9 Å) from the *Tetrahymena thermophila* 40S led to a definition of the locations and folds of all eukaryote-specific proteins in the

Institut de Génétique et de Biologie Moléculaire et Cellulaire, 1 rue Laurent Fries, BP10142, Illkirch F-67400, France; INSERM, U964, Illkirch F-67400, France; CNRS, UMR7104, Illkirch F-67400, France; and Université de Strasbourg, Strasbourg F-67000, France.

*These authors contributed equally to this work.

†To whom correspondence should be addressed. E-mail: adam@igbmc.fr (A.B.-S.); marat@igbmc.fr (M.Y.)

rRNA expansion segments with proteins (Fig. 3, B and C). Multiple interactions with several proteins, using different binding modes, can be packed within a short single-stranded stretch, as exemplified by a fragment of ES39L (Fig. 3C). The application of such stretches as a platform for protein binding is reminiscent of the assembly of Sm proteins onto the single-stranded Sm-site RNA in spliceosome small nuclear ribonucleoproteins (snRNPs) (16).

Eukaryote-specific clusters. Most eukaryote-specific elements on 60S can be divided among three areas along the ring: at the back of the P and L1 stalks and around the central protuberance (CP) (Fig. 2B). These areas, together with the ES6S-ES3S cluster on 40S, represent the largest concentrations of eukaryote-specific elements. Comparing our yeast 40S structure to the one from *T. thermophila* reveals only minor, mostly species-specific, differences in rRNA structure and protein fold (10). Therefore, as the small subunit ES6S-ES3S cluster was previously described (9, 10), we focus here on the three 60S clusters.

Concentration of eukaryotic elements at the back of the P stalk. ES39L emerges from the back of the large subunit at the P-stalk side (Fig. 2B and Fig. 4A) where, together with a eukaryote-specific α helix in L3, it forms one of the contact sites for the signal recognition particle that targets ribosomes to the endoplasmic reticulum membrane (17). The three rRNA helices that constitute ES39L are linked by three stretches of single-stranded rRNA that provide a platform for binding several proteins. The contact between ES39L and its neighboring expansion segment ES7L is mediated by an A-minor interaction where the adenosine stack is donated by ES39L, thereby supporting the idea that the A-minor motif indicates the relative age of its components (fig. S9) (18, 19).

The long bent helix of ES7L encircles L14e and forms extensive interactions with eukaryote-specific proteins and with extensions in conserved proteins (Fig. 4A). The tip of the ES7L helix lies in close proximity to and probably interacts with protein P0, a part of the P stalk that participates in recruiting G proteins to the ribosome (20).

Additional binding partners of ES39L include two core proteins, L3 and L6, with domains in proximity to the sarcin-ricin loop (fig. S10)—an element important in the association of G proteins with ribosomes. Furthermore, L3 plays a role in coordinating the processes of accommodating the aminoacyl-tRNA in the peptidyl-transferase center (PTC) (21), and L6 lines the binding pocket for eukaryotic elongation factor 2 (eEF2;EF-G in bacteria) (22). Thus, ES39L links to functional centers of the ribosome.

Interactions of L6 with protein L14e illustrate a recurrent theme in the yeast ribosome: binding of eukaryote-specific protein elements to conserved ones through interprotein shared β sheets (Fig. 4B). Because these interactions are medi-

ated by the backbones of the two proteins, they pose weak constraints on the sequence of the new element.

Concentration of eukaryotic elements at the back of the L1 stalk. A cluster of four rRNA expansion segments—ES20L, ES26L, ES19L, and ES31L—is located at the back of the L1 stalk (Fig. 2B and Fig. 4C). Both ES20L and ES26L contain a long, narrow, strongly bent loop. The two loops run parallel to one another, forming multiple noncanonical base pairs and stacking interactions (fig. S11). ES31L, which occupies a central position in the cluster, is located opposite the 40S mRNA exit site and forms part of the intersubunit bridge eB8. It is physically anchored to the base of the L1 stalk, a mobile element that plays a role in evacuating the exit-site tRNA (23), and this connection is reinforced via the C-terminal helix of L8e (Fig. 4C). ES31L contains two helices separated by a rRNA single-stranded stretch, 10 residues in length, that serves as a platform for protein-RNA interactions (Fig. 4, C and D). The cluster of expansion segments harbors several eukaryote-specific proteins as well

as the eukaryotic extension of core protein L23, a major component of the “universal docking site” for factors involved in cotranslational targeting, processing, and folding of the nascent chain (Fig. 4C and fig. S12).

Enhanced central protuberance. The CP, dominated by 5S rRNA and its surrounding proteins, establishes the conserved physical contacts, or bridges, between the large subunit and the head of the small subunit. These contacts undergo the most drastic rearrangement during the rotation of the small subunit and swiveling of its head (9). Because the CP also interacts with functional sites on the large subunit, a role in coordinating the activities on the two subunits was proposed (9, 24, 25). In eukaryotes, the CP has several additional elements, and its network of interactions with functional sites on the large subunit is considerably expanded (Fig. 4, E and F). An important contribution to this network is due to protein L20e, which forms a junction where multiple RNA elements, including the dynamic P stalk and 5S, and several different proteins meet. The seven proteins that

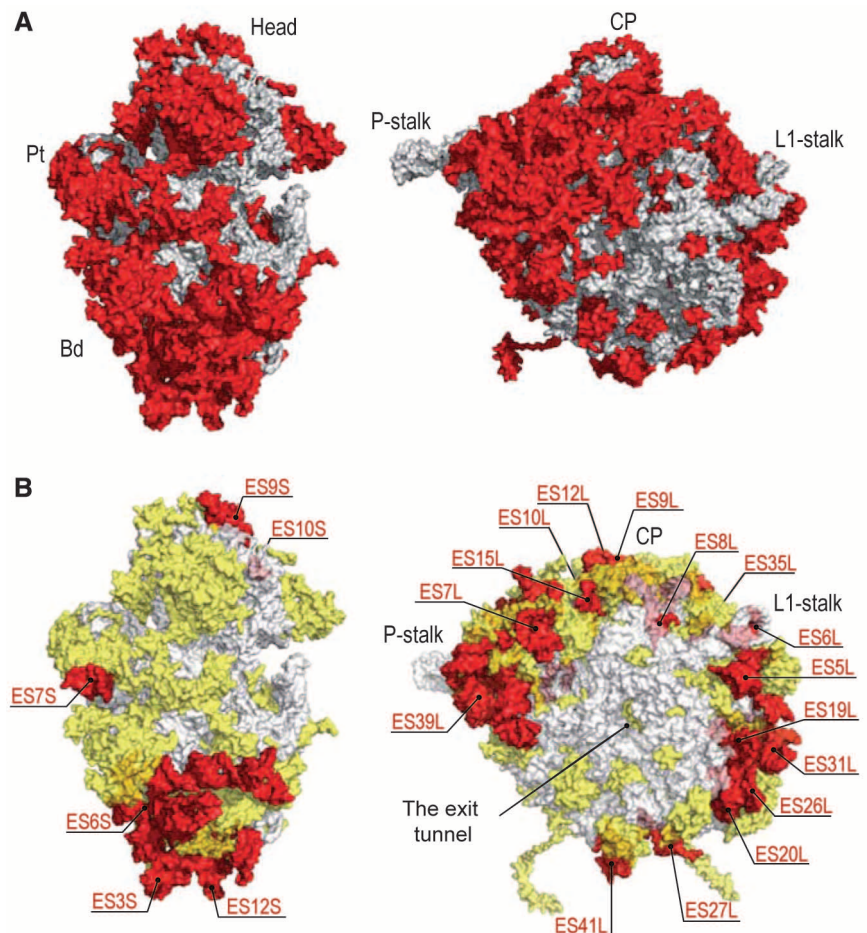


Fig. 2. Characteristics of the 80S ribosome surface. (A) Abundance of eukaryote-specific elements (in red) on the solvent-side of both subunits. Conserved core elements are in gray. Most of the ribosome surface is eukaryote-specific. (B) Distribution of eukaryote-specific protein moieties (yellow) and rRNA expansion segments (red) around the conserved core (gray). Views are of 40S from the back and of 60S from the back through the peptide exit tunnel. Protein moieties are represented by semitransparent surfaces so that all rRNA expansion segments can be seen.

bind L20e include components of core functional centers that are located far apart (Fig. 4, A and E).

The main rRNA additions to the CP are due to ES9L, which consists of two coaxially stacked

helices (partially present in archaea) and to ES12L, which emerges from the base of H38 (Fig. 4E). These elements run parallel to 5S rRNA and squeeze between them the C-terminal helix of the eukaryote-specific protein L29e, whose

N-terminal domain wiggles through the rRNA core to reach the vicinity of the PTC and the base of H89.

Eukaryote-specific bridges. The contact points between the two subunits play an important

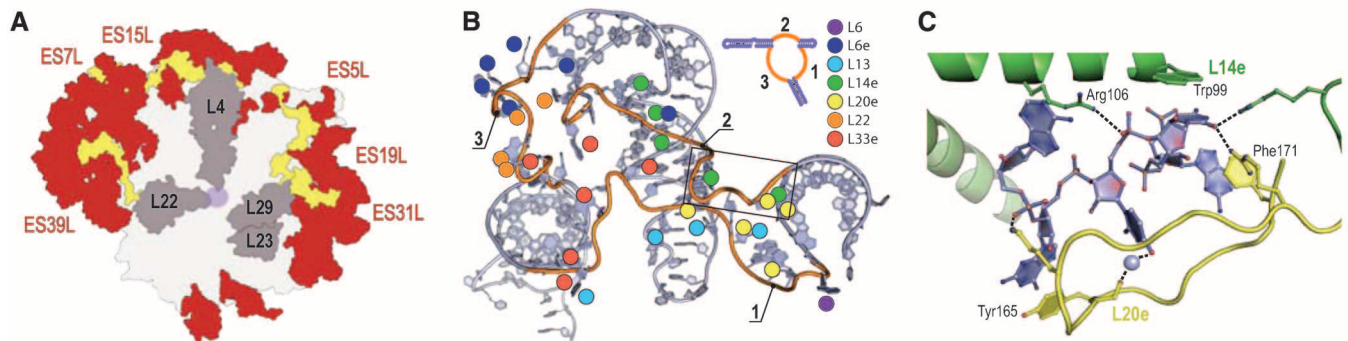


Fig. 3. Features of the rRNA expansion segments. **(A)** Extensions (in yellow) of conserved exit tunnel proteins (gray) associate with rRNA expansion segments (red). View of 60S is as in Fig. 2B, with the position of the exit tunnel rim represented by a purple circle near the center. **(B)** The structure of ES39L, colored according to its two-dimensional diagram (upper right), shows irregular single-stranded rRNA elements (orange) and indicates residues within these

stretches whose exposed bases form interactions with surrounding proteins (circles colored according to interacting protein). A rectangular frame is drawn around the segment shown in **(C)**. **(C)** Multiple interactions between proteins and a single-stranded rRNA stretch. A short fragment of ES39L (blue) interacts with L20e and L14e. Protein residues that stack with exposed bases are labeled; hydrogen bonds are represented by dotted lines.

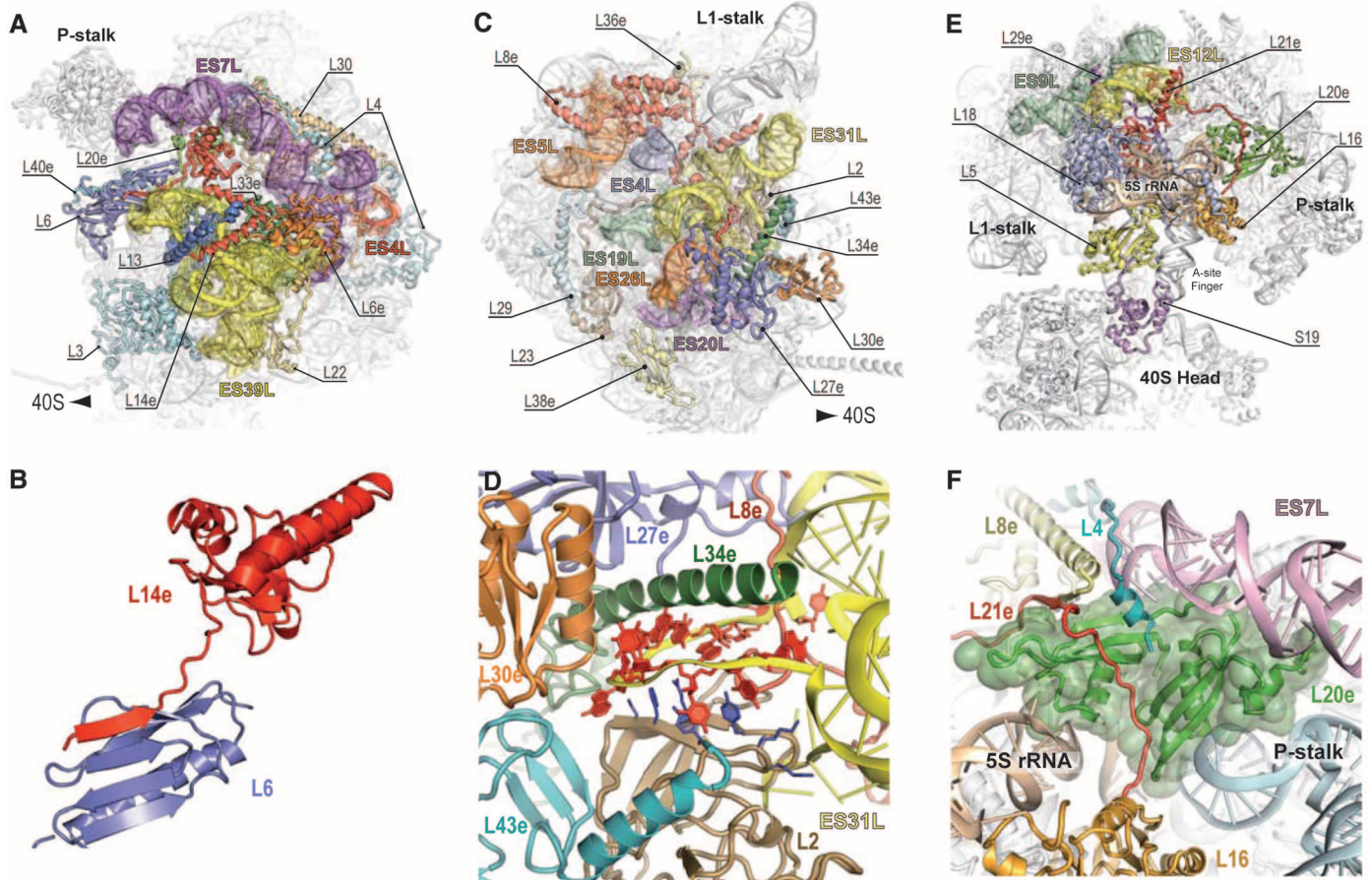


Fig. 4. Concentrations of eukaryote-specific elements along the 60S ring. **(A)** and **(B)** The back of the P stalk: **(A)** overview; **(B)** interprotein β sheet between the conserved L6 and the eukaryote-specific L14e. **(C)** and **(D)** The back of the L1 stalk: **(C)** overview; **(D)** the single-stranded stretch of ES31L (red) as a platform for protein-RNA interactions. Side chains of a structurally conserved domain in

L2 that bind the eukaryotic rRNA element are depicted in blue. There are considerable differences in the sequence of this domain between yeast and bacteria. Evolution of conserved domains, as illustrated here, might result from the addition of eukaryote-specific elements. **(E)** and **(F)** The central protuberance region: **(E)** top view; **(F)** L20e forms multiple interactions with RNA and proteins.

structural role, in addition to transmitting information between the subunits and helping to coordinate their activities. The interaction surface between the two subunits is nearly doubled in eukaryotes because of the formation of additional bridges (Fig. 5A). In virtually all the added bridges, nearly all the participating components on both subunits are eukaryote-specific. Proteins play the dominant role in forming the eukaryote-specific bridges, in sharp contrast to bacteria (26).

We describe here the molecular details of all major eukaryote-specific bridges (Fig. 5, figs. S13 and S14, and table S5).

Bridge eB8 is constructed by the eukaryote-specific protein S1e, which defines the far end of the 40S platform and ES31L (Fig. 5, B and C). In ribosome A, the bridge is formed via long-range interactions that are mediated by either positive ions or water molecules positioned between aspartates of S1e and phosphate groups of ES31L.

The eukaryote-specific bridges are located at the periphery of the ribosome, where rotation of the small subunit results in large shifts. Hence, adaptation of the bridges to different states of the ribosome requires considerable structural plasticity of their components, as illustrated here by ES31L (Fig. 5B).

Just as the 60S component of bridge eB8, namely ES31L, is structurally linked to functionally important domains (Fig. 4C), so are

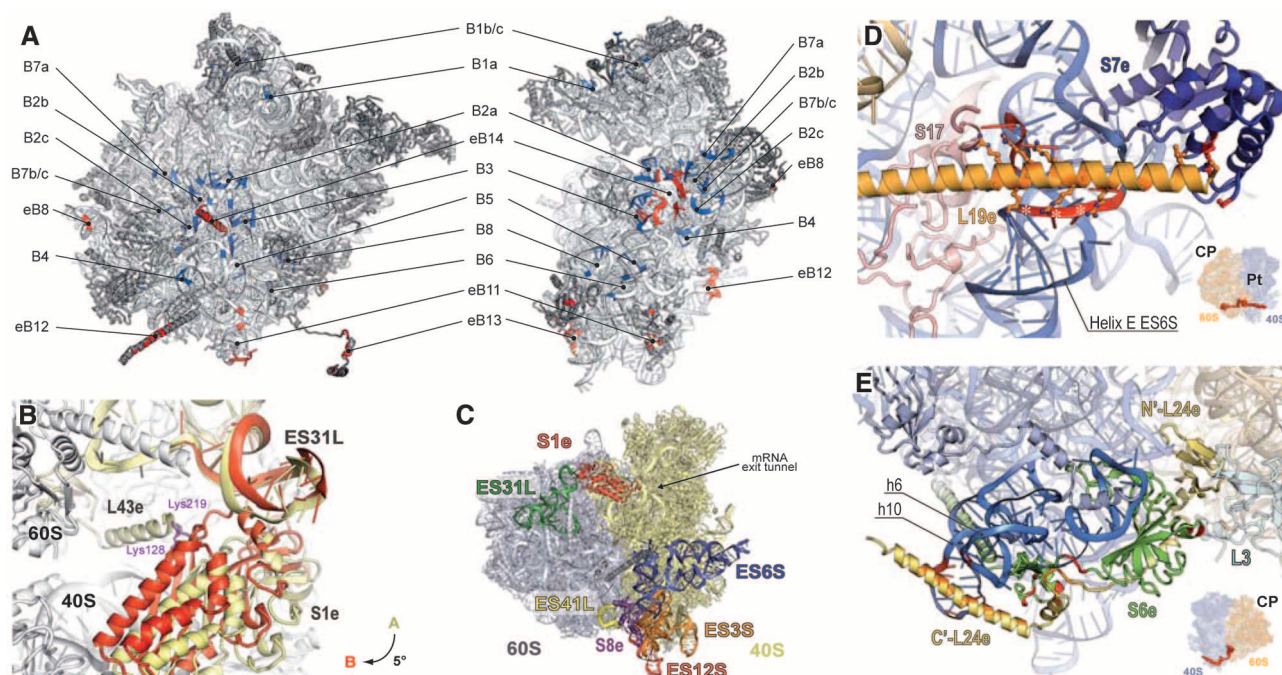


Fig. 5. Intersubunit bridges. **(A)** Interface view showing residues forming eukaryote-specific bridges (red) and conserved ones (blue). **(B)** Rearrangement of bridge eB8, showing the bridge in ribosome A (yellow) compared to that in ribosome B (red). **(C)** The location of bridge eB8 in proximity to the mRNA exit tunnel (arrow) and the location of bridge eB11 within a continuum of eukaryote-specific elements at the bottom of 80S. **(D)** Protein L19e is involved in forming

bridge eB12. Residues of L19e that contact ES6S are shown as sticks. Asterisks (along red ribbon) highlight ES6S residues in proximity to the eIF4G binding site (29). **(E)** L24e extends from the 60S body to interact with S6e on the small subunit. In **(D)** and **(E)**, rRNA and protein residues involved in forming the bridges are in red and orange in 40S and 60S, respectively. Lower right corners show locations of the corresponding bridges within 80S.

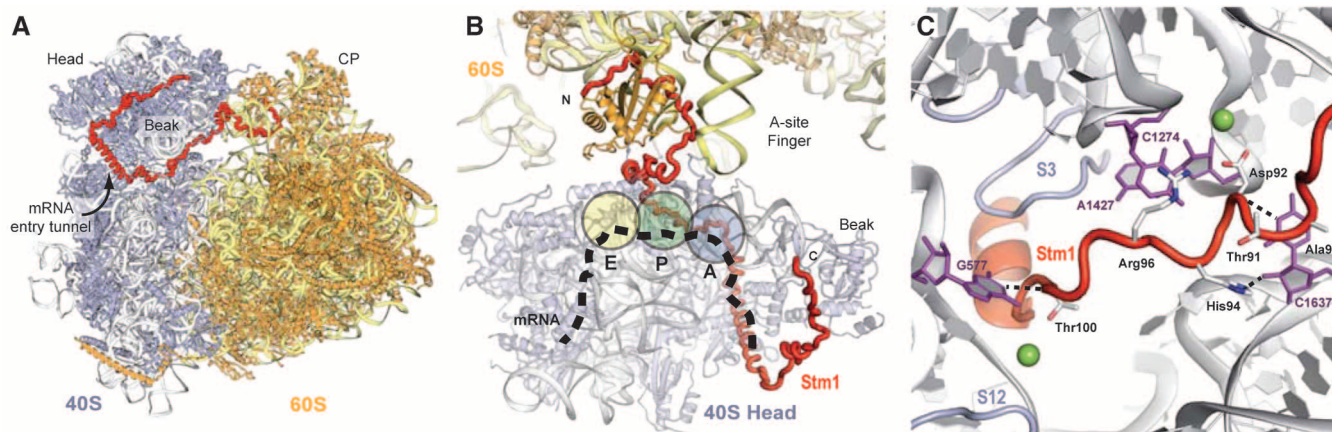


Fig. 6. Stm1 interacts with both subunits and prevents mRNA binding. **(A)** Stm1 (red) binds to 40S (blue) and 60S (yellow). **(B)** Top view of the 40S head and the CP of 60S, showing how Stm1 follows the mRNA pathway until the P site. Dashed black line represents the path of mRNA ac-

ording to crystal structures of bacterial ribosomes (38). Rough locations of A-, P-, and E-tRNA sites are indicated. **(C)** Stm1 interacts with conserved rRNA residues (magenta) that bind mRNA or tRNA in functional complexes.

components on the 40S side. Protein S1e interacts directly with h26, S11, and S26e, which form part of the mRNA exit tunnel (Fig. 1 and Fig. 5C). Furthermore, cross-linking experiments resolved interactions between hepatitis C virus (HCV) internal ribosome entry sites (IRES) and protein S1e (27). Indeed, docking our 80S model into cryo-EM maps of the HCV IRES attached to human ribosomes (28) reveals that one of its contact sites on the ribosome is established by protein S1e.

Protein S8e is sandwiched between ES3S on the small subunit and ES41L on the large subunit, thus creating bridge eB11 (Fig. 5C and fig. S13). ES3S is part of the expanded network of interaction at the bottom of the small subunit that includes ES6S, making S8e a link in a large continuum of eukaryote-specific elements, ~100 Å in length, that begins on the platform of the small subunit, just below the mRNA exit tunnel where ES6S emerges (Fig. 5C).

The only eukaryote-specific bridge positioned at the center of the ribosome is bridge eB14 (fig. S14). The bridge is formed by protein L41e, which consists of a single α helix that is enveloped by conserved core rRNA. L41e protrudes from 60S into a binding pocket in the small subunit, which is lined by helices h27, h45, and h44, in proximity to the decoding center. Curiously, in the context of the full ribosome, L41e is much more strongly associated with 40S than with 60S.

Bridges contacting 40S from the side. A distinctive feature of the eukaryotic large subunit is two long protein helices extending from its left and right sides. These helices—eukaryote-specific additions to proteins L19e and L24e—create two bridges, eB12 and eB13 respectively, that are not buried within the intersubunit interface and are accessible from the solvent.

Bridge eB12 appearing below the mRNA exit tunnel is mainly formed through multiple interactions between several turns of the C-terminal α helix of L19e and the base of helix E in ES6S (Fig. 5D). The major part of the small-subunit side of this bridge is established by ES6S residues that were shown to lie in close proximity to the binding site for eIF4G, a protein that plays a central role in assembling the pre-initiation complex (29). This suggests involvement of eB12 and L19e in the last stages of translation initiation, in particular, subunit joining and shedding/releasing factors.

Protein L24e consists of an N-terminal domain that resides in 60S, followed by a long flexible linker that protrudes deep into the side of the 40S body and a C-terminal domain that reaches the back of 40S (Fig. 5E). The strong interactions of the C-terminal part of L24e with S6e and h10 constitute the bulk of bridge eB13. Comparison of ribosomes A and B suggests that the L24e C-terminal domain follows the movements of 40S, a feature facilitated by the protein's flexible linker, as if it were a bona fide 40S component. This architecture of L24e should be considered in

light of the finding that L24e is a key player in translation re-initiation of polycistronic mRNAs and that its C-terminal domain mediates retention of eIF3 on the ribosome, a necessary condition for re-initiation (30–32).

The C-terminal helix of S6e harbors serines phosphorylated by S6K1 of the TOR pathway (33) and reaches the vicinity of ES6S helix B on the back of 40S (fig. S15). Taking into account the fact that we are missing the last 10 residues of the S6e C terminus, the structure raises the possibility that S6e interacts with factors that dock on ES6S or are involved in initiation or re-initiation.

Stm1. Previous studies have shown that protein Stm1 can associate with full ribosomes and inhibit translation, but the nature and role of these interactions was unknown (34, 35). We find that Stm1 binds the head domain of 40S and precludes mRNA access by inserting an α helix through the mRNA entry tunnel (Fig. 6A). Furthermore, Stm1 follows the path of mRNA until the P site, contacting conserved residues from the 40S body that play a role in binding mRNA or tRNA at the P and A sites of functional ribosome complexes (Fig. 6, B and C). The protein then crosses to the 60S through interactions mainly with helix H84 and eventually exits 60S between 5S rRNA and protein L5 (Fig. 6A). Along its long path, Stm1 contacts nine different ribosomal proteins—one on 60S, eight on 40S. This conformation of Stm1 clamps the two subunits, prevents their dissociation, and further inhibits translation by excluding mRNA binding. Stm1 was shown to play an important role in yeast recovery after experiencing long periods of nutrient-deficient conditions. Because we purified our ribosomes from yeast grown for a few minutes under glucose starvation conditions (9), we suggest that either Stm1 binding or a conformational change of an already bound Stm1 are induced by such stress. Stm1 might act to preserve ribosomes and inhibit their activity until nutrients are abundant. It is thus a functional analog of prokaryotic and chloroplast stress-induced ribosome preservation proteins (36, 37).

Conclusion. The model presented here provides a molecular description of the complete eukaryotic ribosome. It forms a framework for the design and analysis of further experiments that will shed light on diverse aspects of ribosome function, regulation, and assembly as well as the role of its eukaryote-specific elements.

References and Notes

1. T. M. Schmeing, V. Ramakrishnan, *Nature* **461**, 1234 (2009).
2. R. J. Jackson, C. U. Hellen, T. V. Pestova, *Nat. Rev. Mol. Cell Biol.* **11**, 113 (2010).
3. N. Sonenberg, A. G. Hinnebusch, *Cell* **136**, 731 (2009).
4. C. M. Spahn *et al.*, *Cell* **107**, 373 (2001).
5. O. Lecompte, R. Ripp, J. C. Thierry, D. Moras, O. Poch, *Nucleic Acids Res.* **30**, 5382 (2002).
6. M. Schüler *et al.*, *Nat. Struct. Mol. Biol.* **13**, 1092 (2006).
7. D. J. Taylor *et al.*, *Structure* **17**, 1591 (2009).

8. T. Becker *et al.*, *Science* **326**, 1369 (2009); 10.1126/science.1178535.
9. A. Ben-Shem, L. Jenner, G. Yusupova, M. Yusupov, *Science* **330**, 1203 (2010).
10. J. Rabl, M. Leibundgut, S. F. Ataide, A. Haag, N. Ban, *Science* **331**, 730 (2011); 10.1126/science.1198308.
11. See supporting material on Science Online.
12. W. Zhang, J. A. Dunkle, J. H. D. Cate, *Science* **325**, 1014 (2009).
13. P. Nissen, J. Hansen, N. Ban, P. B. Moore, T. A. Steitz, *Science* **289**, 920 (2000).
14. B. T. Wimberly *et al.*, *Nature* **407**, 327 (2000).
15. N. Ban, P. Nissen, J. Hansen, P. B. Moore, T. A. Steitz, *Science* **289**, 905 (2000).
16. D. A. Pomeranz Krummel, C. Oubridge, A. K. Leung, J. Li, K. Nagai, *Nature* **458**, 475 (2009).
17. M. Halic *et al.*, *Nature* **427**, 808 (2004).
18. K. Bokov, S. V. Steinberg, *Nature* **457**, 977 (2009).
19. P. Nissen, J. A. Ippolito, N. Ban, P. B. Moore, T. A. Steitz, *Proc. Natl. Acad. Sci. U.S.A.* **98**, 4899 (2001).
20. M. Diaconu *et al.*, *Cell* **121**, 991 (2005).
21. A. Meskauskas, J. D. Dinman, *Mol. Cell* **25**, 877 (2007).
22. C. M. Spahn *et al.*, *EMBO J.* **23**, 1008 (2004).
23. A. Korostelev, D. N. Ermolenko, H. F. Noller, *Curr. Opin. Chem. Biol.* **12**, 674 (2008).
24. M. H. Rhodin, J. D. Dinman, *PLoS One* **6**, e20048 (2011).
25. M. W. Smith, A. Meskauskas, P. Wang, P. V. Sergiev, J. D. Dinman, *Mol. Cell Biol.* **21**, 8264 (2001).
26. M. M. Yusupov *et al.*, *Science* **292**, 883 (2001); 10.1126/science.1060089.
27. E. Babaylova *et al.*, *Nucleic Acids Res.* **37**, 1141 (2009).
28. D. Boehringer, R. Thermann, A. Ostareck-Lederer, J. D. Lewis, H. Stark, *Structure* **13**, 1695 (2005).
29. Y. Yu, I. S. Abaeva, A. Marintchev, T. V. Pestova, C. U. Hellen, *Nucleic Acids Res.* **39**, 4851 (2011).
30. H. S. Park, A. Himmelbach, K. S. Browning, T. Hohn, L. A. Ryabova, *Cell* **106**, 723 (2001).
31. T. Nishimura, T. Wada, K. T. Yamamoto, K. Okada, *Plant Cell* **17**, 2940 (2005).
32. O. Thiébeault *et al.*, *EMBO J.* **28**, 3171 (2009).
33. I. Ruvinsky, O. Meyuhis, *Trends Biochem. Sci.* **31**, 342 (2006).
34. N. Van Dyke, J. Baby, M. W. Van Dyke, *J. Mol. Biol.* **358**, 1023 (2006).
35. V. Balagopal, R. Parker, *RNA* **17**, 835 (2011).
36. A. Vila-Sanjurjo, B. S. Schuwirth, C. W. Hau, J. H. Cate, *Nat. Struct. Mol. Biol.* **11**, 1054 (2004).
37. M. R. Sharma *et al.*, *J. Biol. Chem.* **285**, 4006 (2010).
38. L. B. Jenner, N. Demeshkina, G. Yusupova, M. Yusupov, *Nat. Struct. Mol. Biol.* **17**, 555 (2010).

Acknowledgments: We thank C. Schulze-Briese, M. Mueller, and the staff at the Swiss Light Source for advice on data collection strategy; K. Diederichs for guidance on estimating data quality; B. Seraphin and A. Urzhumtsev for invaluable discussions; M. Fournier and V. Chavant for performing mass spectrometry analysis; and S. Uge for assistance with computer facilities. Supported by a European Molecular Biology Organization long-term fellowship (A.B.-S.), the Human Frontier Science Program, French National Research Agency grants ANR BLAN07-3_190451 and ANR-07-PCVI-0015-01, and the European Commission SPINE2. Coordinates and structure factors have been deposited in the Protein Data Bank with accession codes 3U5B, 3U5C, 3U5D, 3U5E, 3U5F, 3U5G, 3U5H, and 3U5I.

Supporting Online Material

www.sciencemag.org/cgi/content/full/science.1212642/DC1
Materials and Methods
Figs. S1 to S15
Tables S1 to S5
References (39–59)

15 August 2011; accepted 4 November 2011
Published online 17 November 2011;
10.1126/science.1212642



Supporting Online Material for

The Structure of the Eukaryotic Ribosome at 3.0 Å Resolution

Adam Ben-Shem,* Nicolas Garreau de Loubresse, Sergey Melnikov, Lasse Jenner,
Gulnara Yusupova, Marat Yusupov*

*To whom correspondence should be addressed. E-mail: adam@igbmc.fr (A.B.-S.); marat@igbmc.fr (M.Y.)

Published 17 November 2011 on *Science* Express
DOI: 10.1126/science.1212642

This PDF file includes:

Materials and Methods

Figs. S1 to S15

Tables S1 to S5

References (39–59)

Materials and Methods

Purification and crystallization of yeast ribosomes. Purification and crystallization followed the same protocol we used previously (9). Yeast strain JD1370 was provided by J. Dinman's lab (U. of Maryland). The L-A virus was eliminated from this strain to avoid contamination of the ribosome preparation due to fragments of viral particles. Yeast grew in flasks to an OD₆₀₀ of 1.45 in YPD at 30°C. Cells were pelleted by centrifugation, re-suspended with YP (i.e. without glucose) and incubated in flasks with vigorous shaking (250 rpm) for 10 minutes (39). All further steps were performed at 0-4°C. Cells were precipitated and washed three times in buffer M (30mM Hepes-K pH 7.5, 50 mM KCl, 10 mM MgCl₂, 8.5% mannitol, 2mM DTT, 0.5 mM EDTA). Following the final centrifugation (3450g * 10 min) the pellet was weighed. Typically we obtained 4.5 gr of cells from 4L of cell culture.

For 4.5 gr of cells, the pellet was resuspended in 6.5 ml of buffer M and supplemented with additional 600 µL from a solution of one complete protease inhibitor tablet (without EDTA, Roche) dissolved in 2 ml buffer M, 100 µL RNasin (Promega), 120 µL Pefablock 100 mM and 56 µL freshly prepared Na-heparin 100 mg/ml (heparin concentrations were found to affect the amount of PEG required at later steps to precipitate the ribosomes). The cell suspension was transferred to a round-bottom 50 ml tube (Nalgene) with 13.5 grams of pre-chilled 425-600 µm glass-beads (Sigma). Cells were disrupted by manually shaking the tube 5 times at a frequency of 3Hz in the cold room for 1 minute with 1 min breaks on ice between each shake (a modified version of (40)).

Beads were removed by short centrifugation (20,000g * 2 min) and the lysate was further clarified by a longer centrifugation (31,000g * 9 min). PEG 20,000 was then added from a 30% w/v stock (Hampton Research) to a final concentration of 4.5% w/v and the solution was left to stand for 5 minutes on ice. The solution was clarified by centrifugation (20,000g * 5 min) and the supernatant was decanted to a new tube. Residual solution was "squeezed" out from the pellet by an additional short 1 min centrifugation. The KCl concentration was then adjusted to 130 mM. After 5 min on ice PEG 20,000 concentrations were adjusted to 8.5% and the solution was left to stand for 10 min on ice. Ribosomes were precipitated (17,500g * 10 min), the supernatant was discarded and residual solution was removed by a short spin of the pellet (14,500g * 1 min). Ribosomes were suspended (6.5-7 mg/ml) in buffer M2 (buffer M with KCl concentration adjusted to 150 mM and supplemented with protease inhibitors and heparin). Typically 32-35 mg of ribosomes were obtained from 4.5g of yeast cells.

Ribosomes were further purified by a 15-30% sucrose gradient in buffer A (20 mM Hepes-K pH 7.5, 120 mM KCl, 8.3 mM MgCl₂, 2 mM DTT, 0.3 mM EDTA) using the SW28 rotor (18,000 rpm * 15h). The appropriate fractions were collected, KCl and MgCl₂ concentrations were adjusted to 150 mM and 10 mM respectively, PEG 20% was then added to a final concentration of 7% w/v and the solution was left to stand 10 min on ice. Ribosomes were precipitated (17,500g * 10 min), the supernatant was discarded and residual solution was removed by a short spin of the pellet (14,500g * 1 min). Ribosomes were suspended (20 mg/ml) in buffer G (10 mM Hepes-K pH 7.5, 50 mM KOAc, 10 mM NH₄Cl, 2 mM DTT, 5 mM Mg(OAc)₂). Typically 14-19 mgs of pure ribosomes were obtained from 4.5 gr. of cells.

Best crystals were obtained from ribosomes kept on ice for two-weeks (or longer) before crystallization trials were set.

For crystallization, the ribosome stock (after two weeks on ice) is filtered (0.22µm centrifugal filters, Millipore) and a ribosome solution is prepared containing 5 mg/ml ribosomes, 2.5 mM Hepes-K pH 7.5, 2.5 mM NH₄Cl, 3.33 mM Mg(OAc)₂, 1.6 mM DTT, 0.055 mM EDTA, 2.8 mM Deoxy Big Chap, 40 mM KOAc, 5.5 mM NH₄OAc, 5.5 mM Tris-Acetate pH 7.0. The ribosome solution is incubated at 30°C for 10 min and left to cool down for an hour in the cold room. Ribosomes were crystallized by the hanging drop method at 4°C by mixing 2-2.4 µL of ribosome solution with 1.6 µL of well solution (95 mM Tris-Acetate pH 7.0, 95 mM KSCN, 3 mM Mg(OAc)₂, 19% glycerol, 4-4.5% w/v PEG 20,000, 4.75 mM spermidine). Crystals appeared within 7-10 days and reached their full size after additional two weeks.

Post-crystallization treatment. Modifications to the original dehydration procedure (9) improved the reproducibility and quality of the crystals diffraction. The hanging-drop cover-slip was placed in a small tissue-culture Petri dish (35*10 mm) and the mother liqueur was first replaced by a solution with slightly higher concentration of PEG 20,000 (80mM Tris-Acetate pH 7.0, 70 mM KSCN, 10mM Mg(OAc)₂, 20% v/v Glycerol, 5% w/v PEG 20,000, 6.5 mM spermidine, 7.5 mM NH₄OAc, 1.4 mM Deoxy Big Chap, 2mM DTT). This solution was then replaced step-wise, with 15 minutes breaks between steps, by solutions with increasing concentrations of PEG 6000, reaching finally after five steps to 20% (80 mM Tris-Acetate pH 7.0, 70 mM KSCN, 10 mM Mg(OAc)₂, 18% v/v Glycerol, 5% w/v PEG 20,000, 6.5 mM spermidine, 7.5 mM NH₄OAc, 20% w/v PEG 6000, without DTT, without detergent). This solution was then replaced with the same solution supplemented with 2 mM osmium hexamine and the drop was kept in the Petri dish sealed with parafilm for 30 min-5h. Crystals were frozen directly on the goniometer in the stream of cold nitrogen.

Data collection and reduction. Diffraction data was collected from crystals cooled to 90°K using 0.1° oscillation in beam-line X06SA at SLS. We used a data collection strategy developed at SLS (41) which exploits the unique features of the single photon counting pixel detector PILATUS 6M. The beam was attenuated to roughly 7.5% of its flux so that radiation damage could be significantly reduced and a highly redundant data-set could be collected using several crystals and multiple spots per each crystal. Data was reduced by the XDS suite (42) and Truncate (43) yielding the statistics displayed in Table S1.

Map calculation, model building and refinement. The 4.15Å resolution model (9) was used as a starting point for our efforts to build a full 80S structure at a higher resolution. This initial model was improved by several rounds of rigid body refinement in Phenix (44), starting with one body per 80S and ending with 5 (large subunit, head, body, platform, penultimate stem-loop). The model was further improved by simulated annealing refinement of individual atom coordinates and single B-factor per residue applying NCS restraints (between domains and single proteins) as well as secondary structure restraints for proteins and base-pair restraints for rRNA. The refined initial model was used to locate roughly 1400 osmium hexamine sites using Phaser (45). The calculated SAD phases, either alone or combined with model phases, were improved by density modification in PARROT (46) or SOLOMON (47) as implemented in CNS (48). The density modified maps guided manual model building in COOT (49) and showed clear density for most rRNA bases and protein side chains. RNA chains of the initial refined model were corrected and proteins with homologues in prokaryotic ribosomal structures were re-traced and side-chains modeled. Proteins with no homologues in prokaryotic ribosomal structures were first identified according to their size, fold, unique features such as zinc finger and finally by the fit between their sequences and the electron density. Several rounds of model building, refinement and map improvements ensued. The final refinement did not use simulated annealing and applied tight geometry restraints. NCS restraints were not applied in the last round of refinement.

Analysis. Electrostatic potential analysis of the 40S and 60S surfaces was performed with APBS (50) using an interface provided by VMD (51). Solvent exposed surface was determined by AreaIMol in CCP4 (43). Defining evolutionarily conserved and eukaryote-specific regions within ribosomal proteins was done using structural alignment between the yeast and *E. coli* or *H. marismortui* homologues in FatCat (52). Figures were prepared by PyMol (53). Figures describing the overall structure of the ribosome (Figs. 1 and 2) show ribosome A. The tip of the L1 stalk is missing in our structure but was placed in these figures as one of the important landmarks in the overall ribosomal architecture. The model for the L1 tip was taken from our previous lower resolution model (9). Protein L11 and the C-terminal alpha-helix of L24e have

poor densities in ribosome A and were therefore taken from ribosome B. It is noteworthy that in ribosome A the C-terminal alpha-helix of L24e was displaced from its contact site with 40S by an adjacent ribosome to form a significant crystal contact. We strongly believe that the interaction of this alpha-helix with 40S is maintained in both conformational states (i.e. in ribosome A and B) in solution.

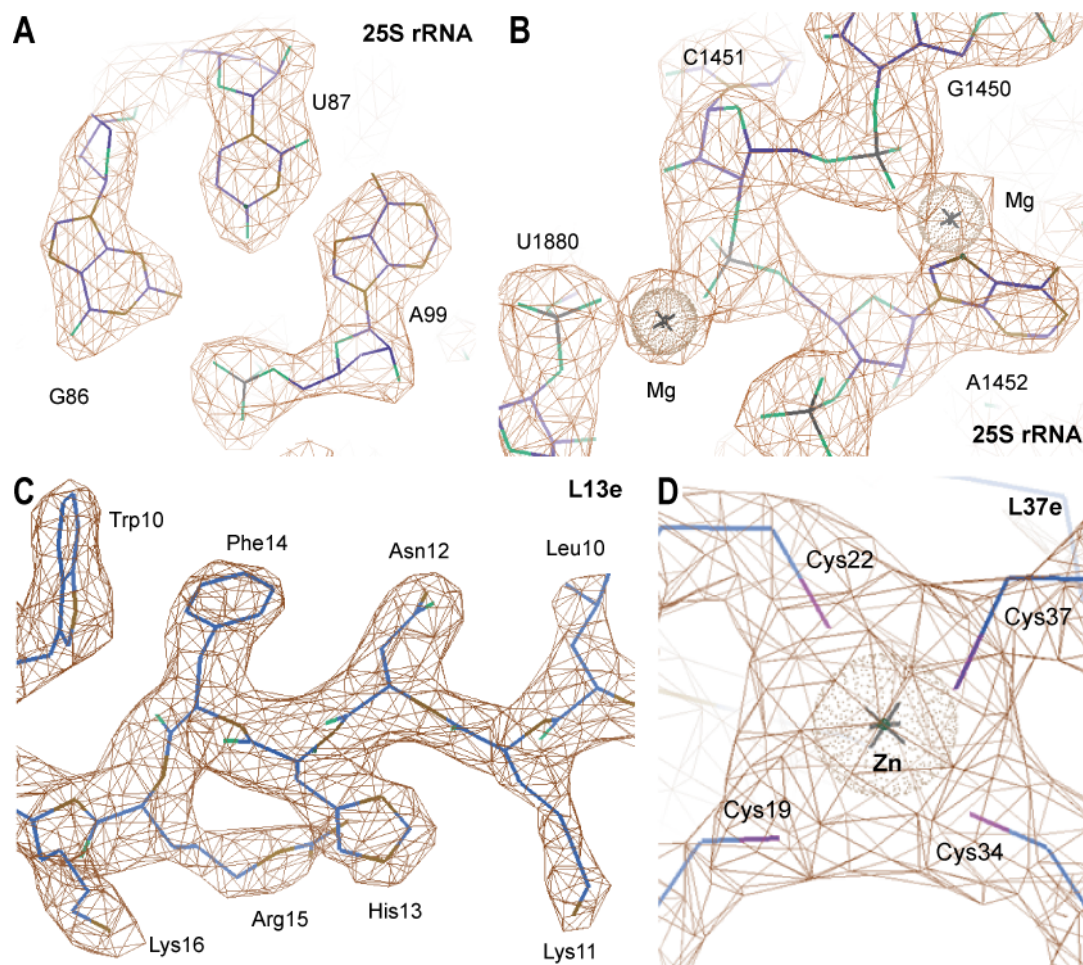
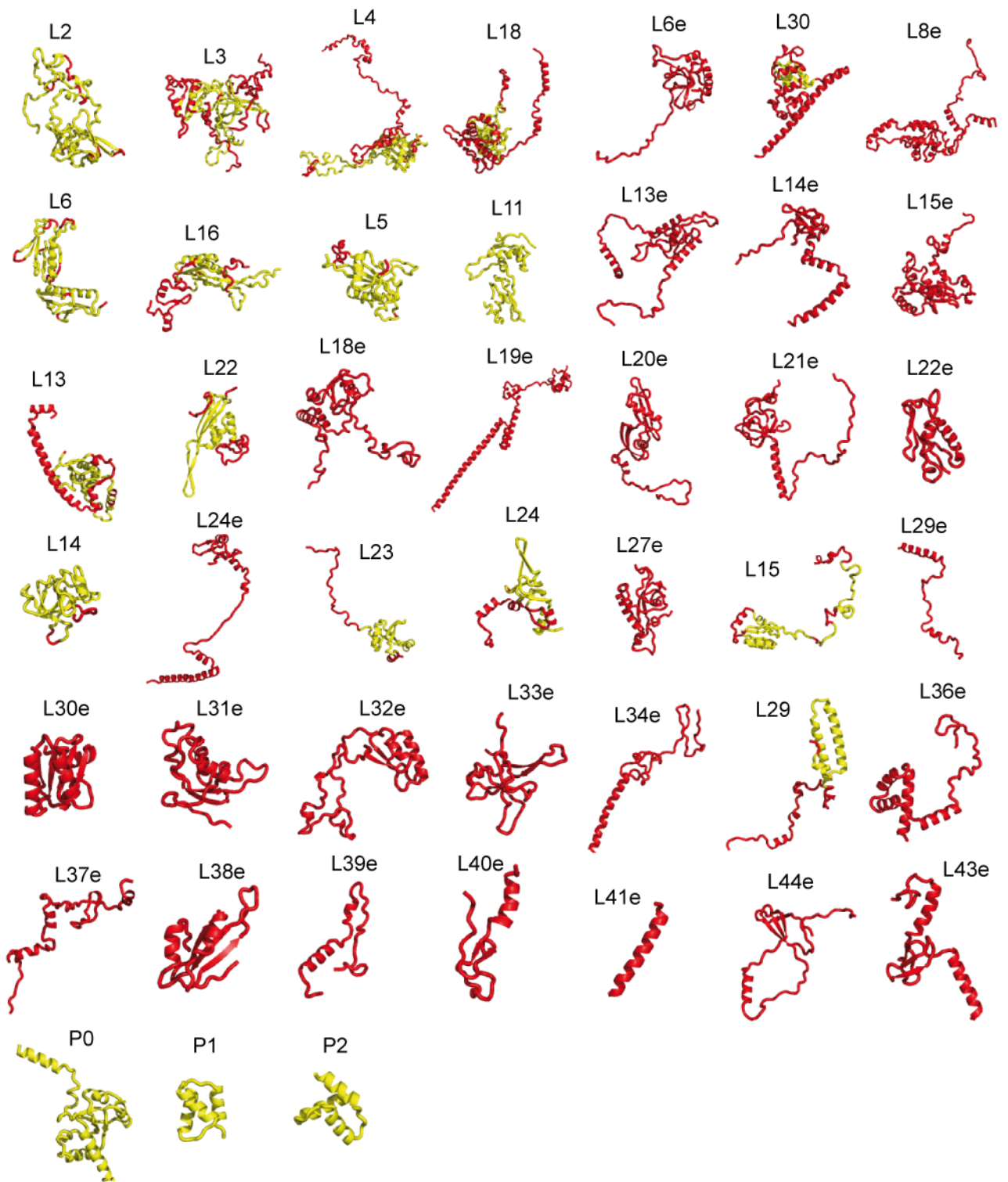


Fig. S1. Representative electron density maps. **(A)** $2F_o-F_c$ map contoured at 1.6σ is shown around residues from 25S and demonstrating that it is possible to distinguish between pyrimidines and purines. **(B)** $2F_o-F_c$ map contoured at 1.6σ showing interactions of magnesium ions with phosphates and bases. **(C)** $2F_o-F_c$ map contoured at 1.0σ is shown around residues from protein L13e. The density for the side chains is clearly visible. **(D)** $2F_o-F_c$ map contoured at 1.0σ is showing the zinc binding pocket in the zinc-finger protein L37e.

Fig. S2. Structural alignment allows better definition of the conserved core in ribosomal proteins. Illustrated by the case of protein S4. **(A)** Multiple sequence alignment of S4 from 6 bacterial species, *Isosphaera pallida* (UniProt identifier: E8R482), *Gloeobacter violaceus* (Q7NFF4), *Clostridium perfringens* (Q8XHV0), *Kosmotoga olearia* (C5CGH5), *Spirochaeta thermophila* (E0RQA5), *Escherichia coli* (P0A7V8), and 6 eukaryotic species (*Saccharomyces cerevisiae* (O13516), *Tetrahymena thermophila* (E6PBS7), *Arabidopsis thaliana* (Q9LXG1), *Dictyostelium discoideum* (F0ZF46), *Homo sapiens* (P46781), *Giardia lamblia* (A8BKS8)). Alignment shows that protein S4 from *S. cerevisiae* contains several short eukaryote-specific insertions (highlighted by red rectangles). **(B)** Structure of S4 from *S. cerevisiae*. Eukaryote-specific insertions are defined and colored according to (A) in red. **(C)** Structural alignment of S4 from *E. coli* (PDB ID 3I1M) and *S. cerevisiae* by FATCAT reveals the structurally conserved core of S4 (in blue) and eukaryote- and bacteria-specific insertions (in red and green respectively). **(D)** Multiple sequence alignment of S4, rearranged according to the structural alignment in (C), illustrates the correct positions of eukaryote- and bacteria-specific insertions within the sequences.



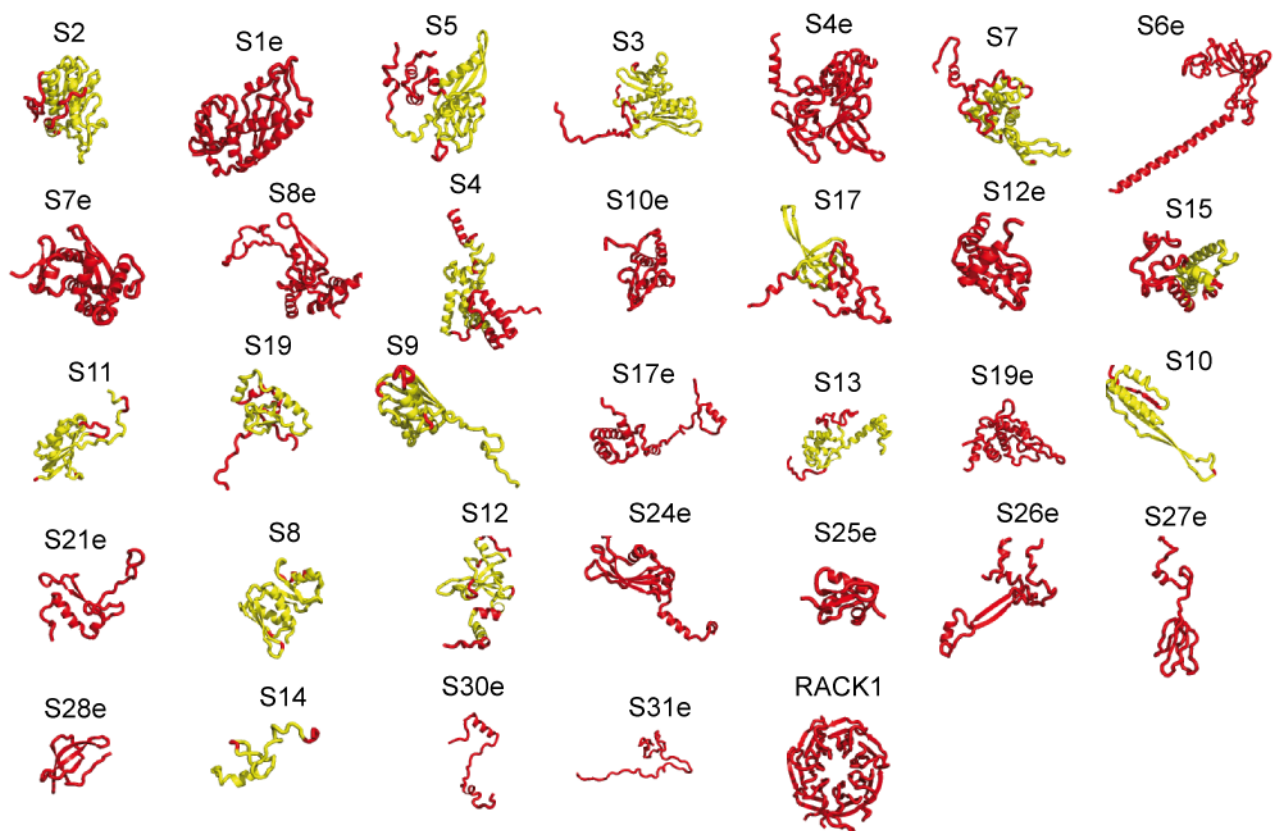


Fig. S3. Structure and conservation of all *S. cerevisiae* ribosomal proteins with the single exception of L1. Domains that are shared by yeast and bacteria, as defined by structural alignments between protein homologues from *S. cerevisiae* and *E. coli* (12), are depicted in yellow. Extensions or proteins that are not found in bacteria are depicted in red.

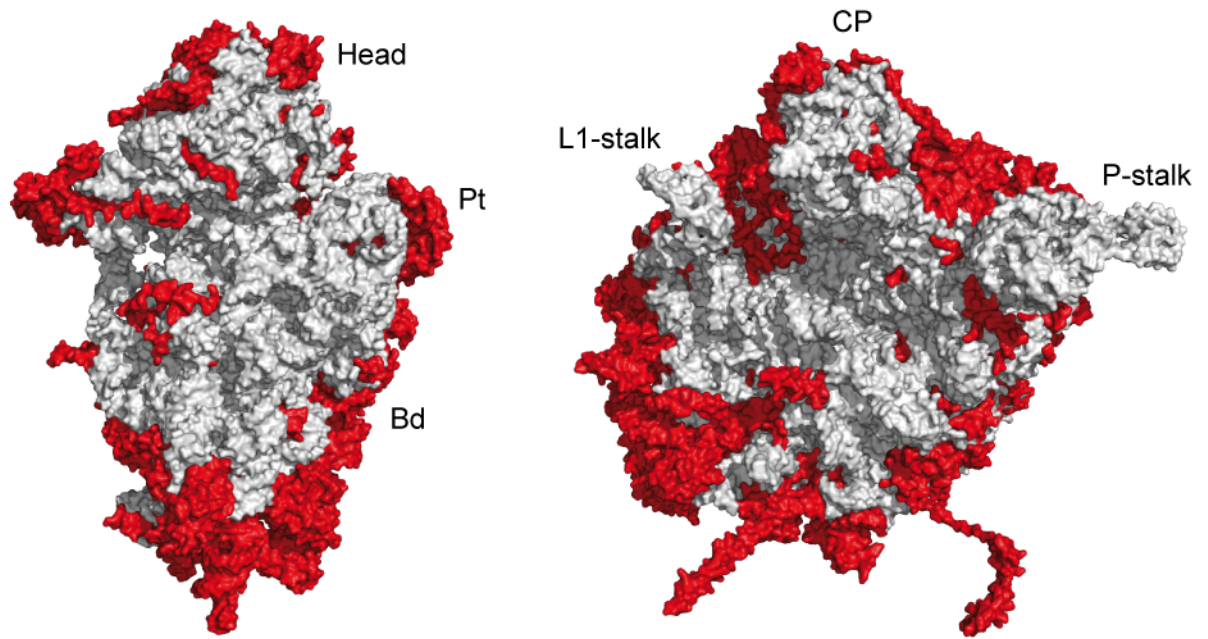


Fig. S4. Paucity of eukaryotic specific elements (red) on the interface side of both subunits. Conserved core elements are in grey.

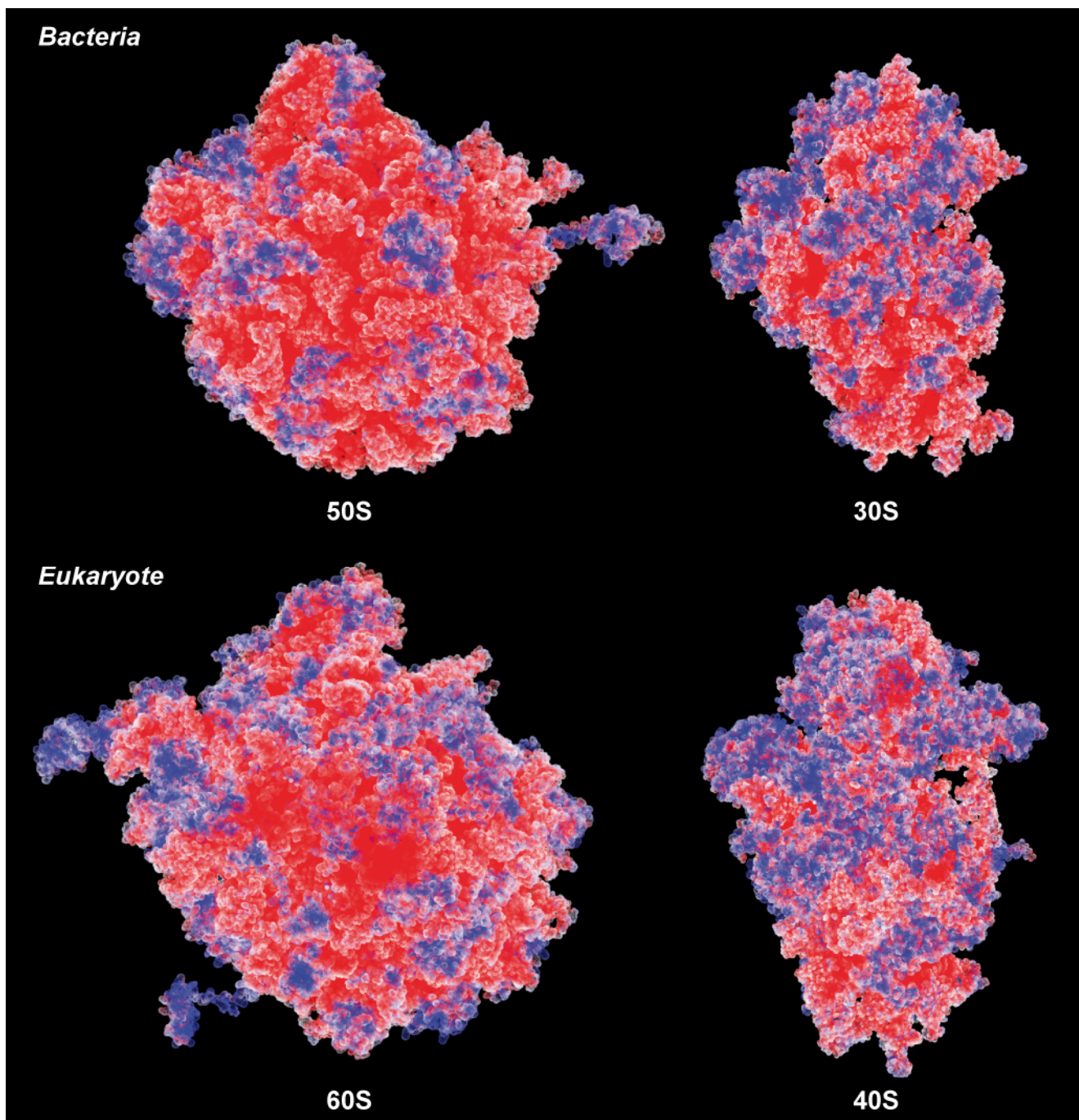


Fig. S5. Electrostatic surface potential of the ribosome. A comparison between yeast and *E. coli* (12). The two subunits are viewed from the solvent side. Blue color indicates regions of positive potential whereas red depicts negative potential values.

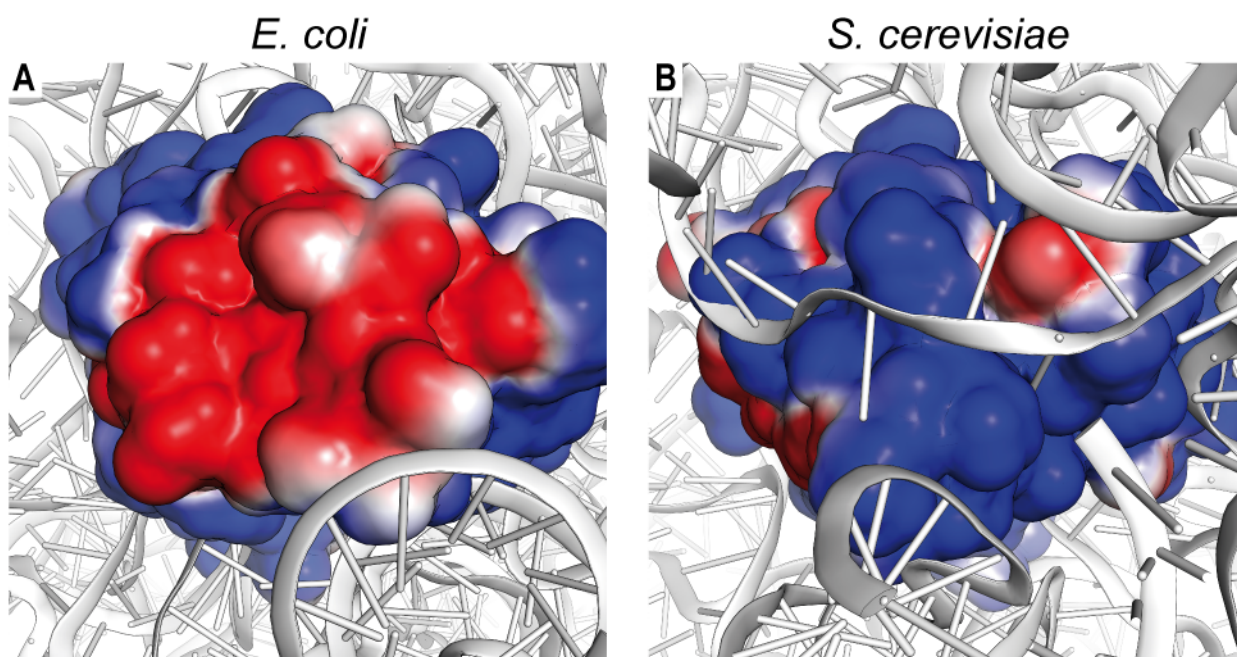


Fig. S6. Differences between *E. coli* (12) and *S. cerevisiae* in the composition of side chains on the surface of conserved proteins. An example of a conserved region (from protein L13, electrostatic potential surface representation) which is exposed to the solvent in bacteria but is covered by a layer of expansion segment rRNA in yeast. The region is dominated by negative residues in bacteria but positive ones in yeast. 23S and 25S rRNAs are in grey.

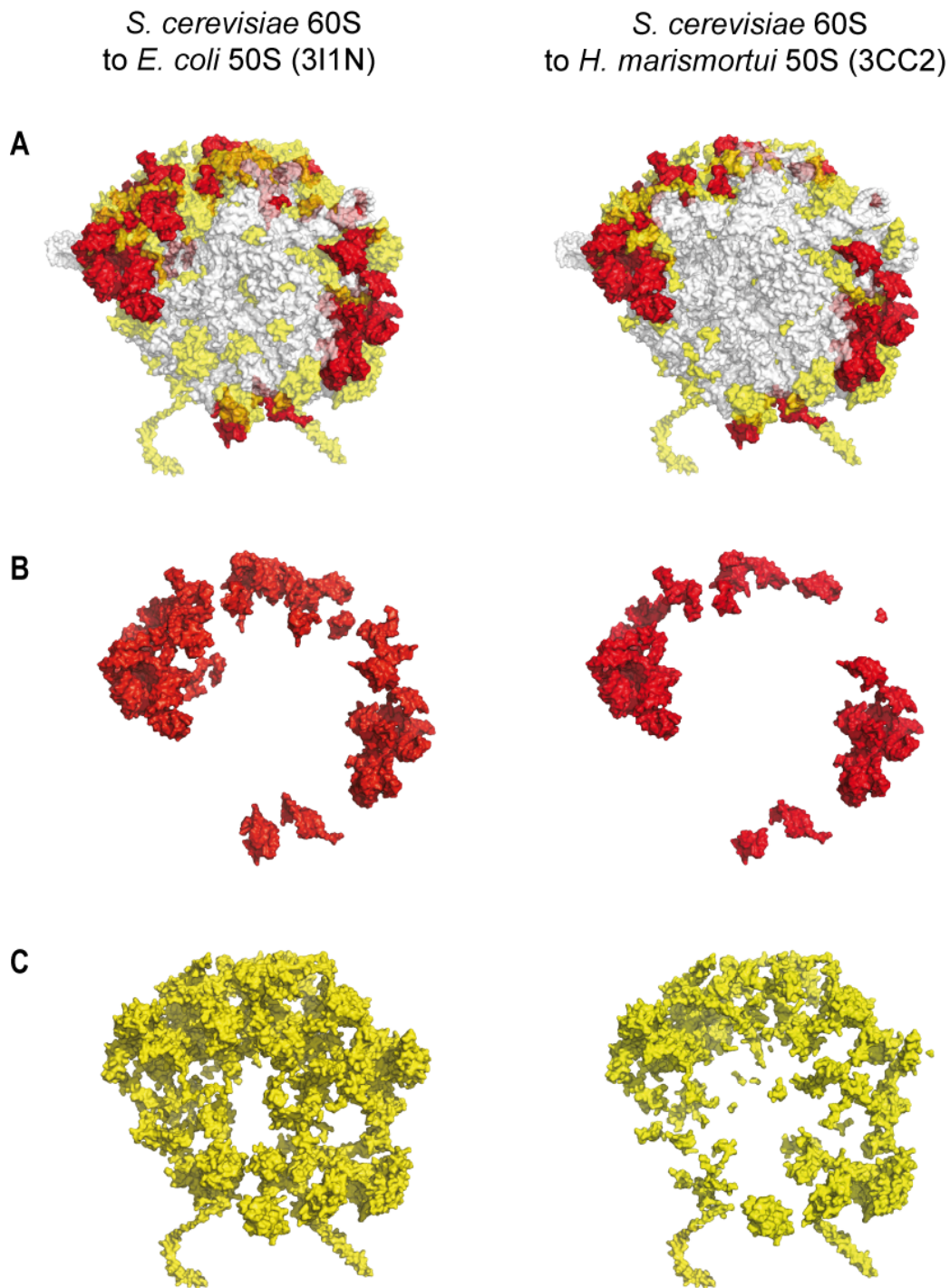


Fig. S7. Comparison of the 60S subunit from *S. cerevisiae* to the 50S subunits from the bacterium *E. coli* (12) and the archaea *H. marismortui* (15). The large subunits are viewed from the back through the peptide exit tunnel. **(A, left)** Distribution of protein moieties (yellow semi-transparent) and rRNA elements (red) that are missing in bacteria around the core shared by bacteria and yeast (grey semi-transparent). **(A, right)** Distribution of protein moieties and rRNA elements that are missing in archaea around the core shared by archaea and yeast (grey semi-transparent). The arrangement of RNA and proteins moieties around the core is similar for both comparisons. **(B)** The ring-like arrangement of rRNA expansions and **(C)** the ring-like distribution of protein moieties. (B and C) are extracted from (A).

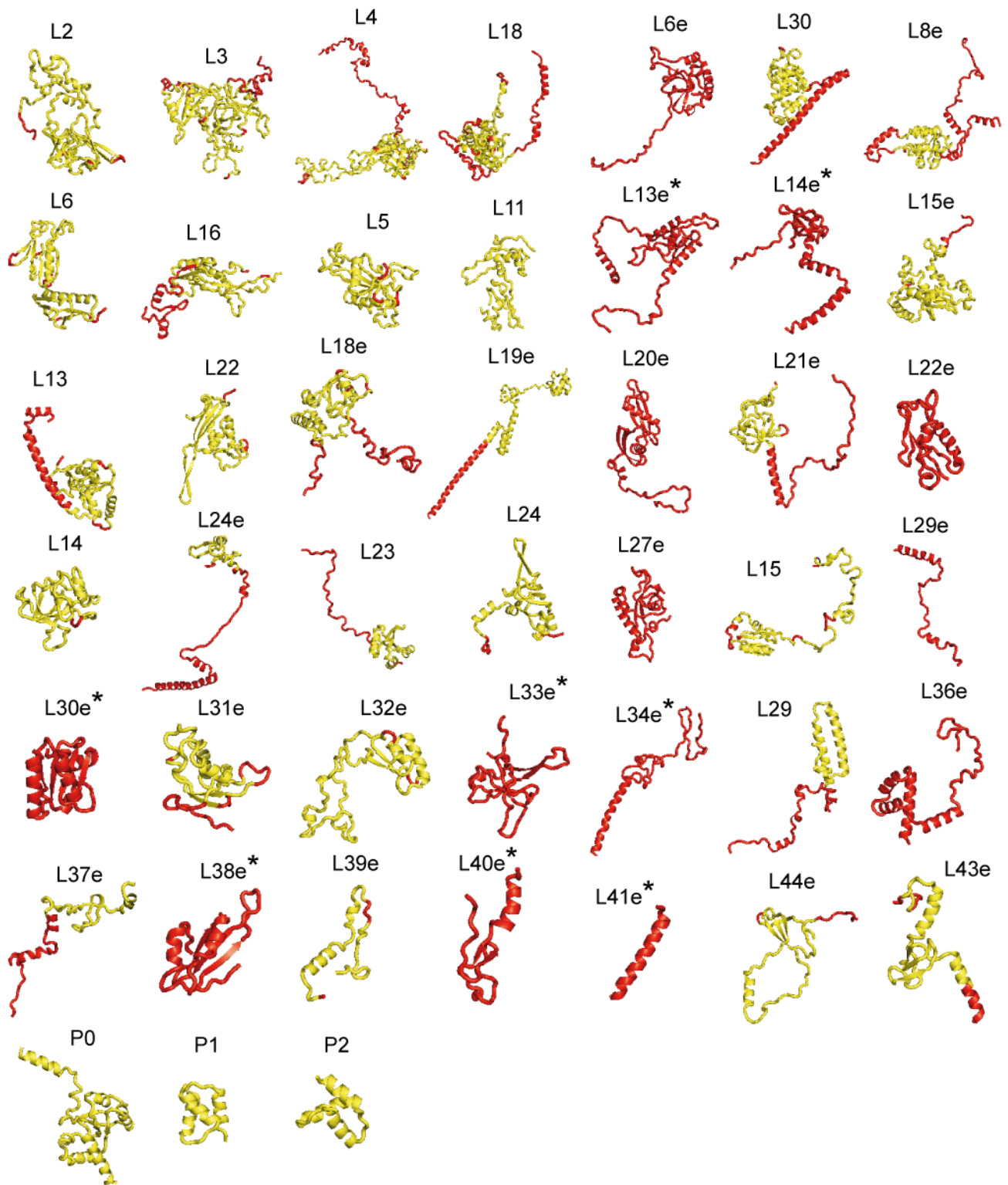


Fig. S8. Structural alignment of large ribosomal subunit proteins from yeast and the archaea *H. marismortui*. Domains shared between yeast and archaea (15) are in yellow. Extensions or proteins not found in *H. marismortui* are in red. The only structure of an archaeal 50S, the one from *H. marismortui*, lacks eight ribosomal proteins that do occur in some other archaea. These eight proteins are labeled with an asterisk.

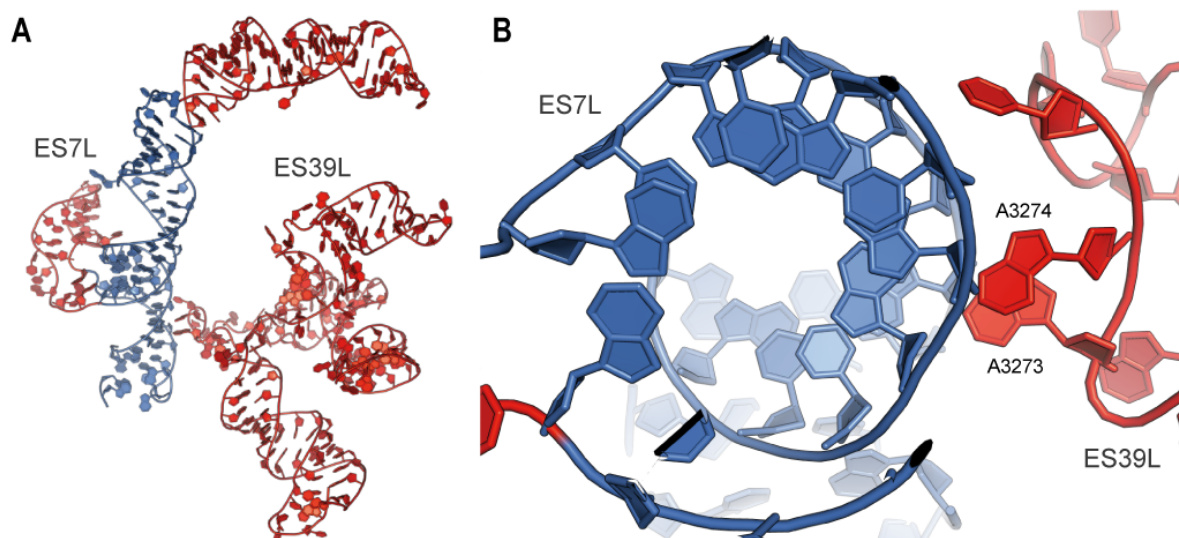


Fig. S9. The A-minor interaction between ES39L and ES7L. **(A)** Side view of the A-minor interactions between ES39L and ES7L **(B)** A closer view on the interaction between ES7L and ES39L. The adenosine stack of A3273 and A3274 bulges out from ES39L and packs with the regular RNA helix at the base of ES7L. The vast majority of rRNA expansion segments, including ES39L, are missing both in bacteria and archaea (depicted in red). However in the structure of the 50S from the archaea *H. marismortui* (15) an RNA helix is found at the position of ES7L's base in yeast (depicted in blue), suggesting that this element preceded the addition of most other expansion segments in evolution. This finding agrees with a recent hypothesis postulating that adenosine stacks should not appear before the corresponding, stabilizing, helix (18).

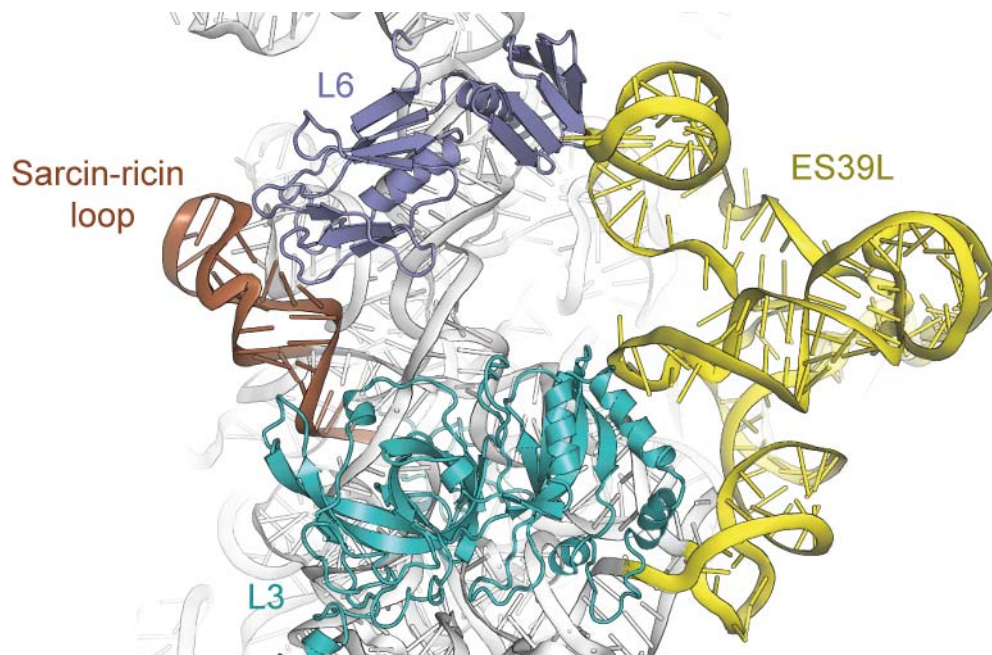


Fig. S10. Side view of the cluster at the back of P-stalk. ES39L interacts with the conserved proteins L3 and L6 that are associated with the sarcin-ricin loop. Other ribosomal proteins are omitted for simplicity. 25S rRNA is in grey.

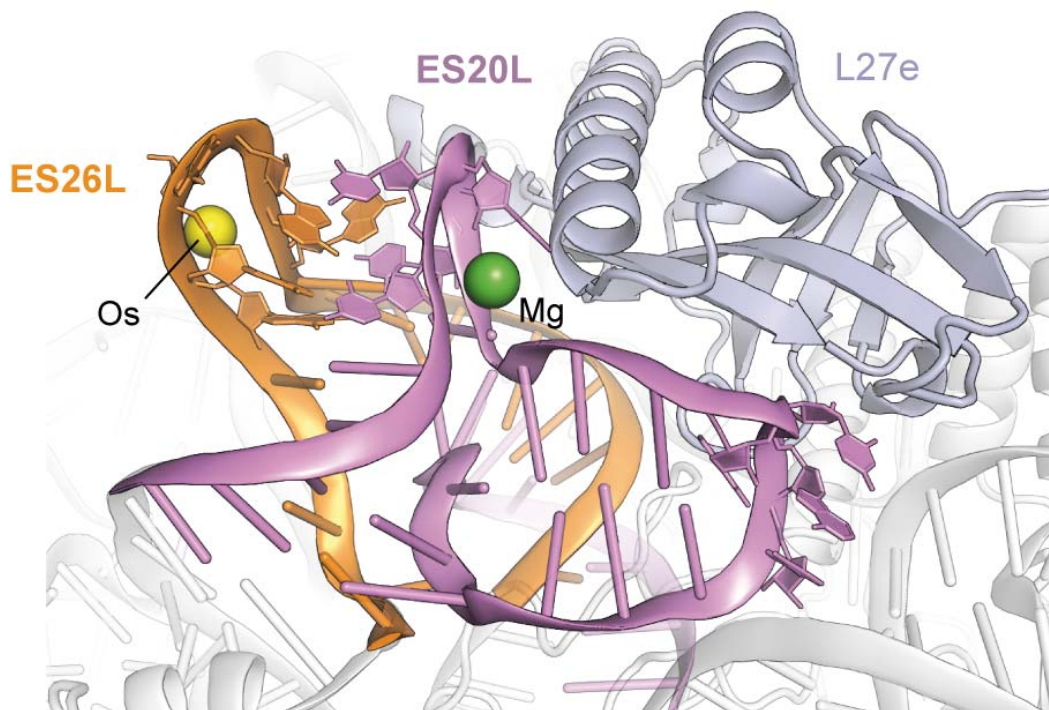


Fig. S11. The uncommon architecture of ES20L and ES26L and the interactions between their strongly bent long loops. Osmium and magnesium ions are represented by spheres.

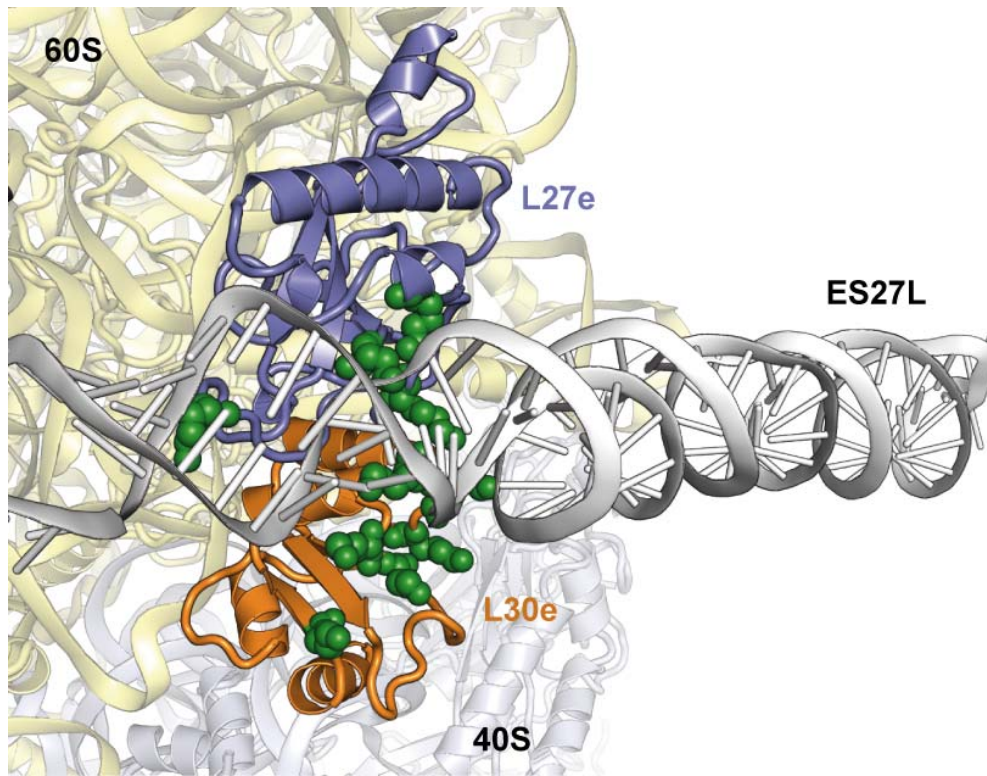


Fig. S12. Proteins L27e and L30e from the concentration of eukaryotic elements at the back of L1-stalk. These proteins present patches of exposed lysines (green spheres) that establish a binding surface for the dynamic and essential expansion segment ES27L which plays a role in coordinating access of various factors to the exit tunnel and the emerging nascent chain (54). A model for ES27L, which is missing from our structure, was taken from (55)

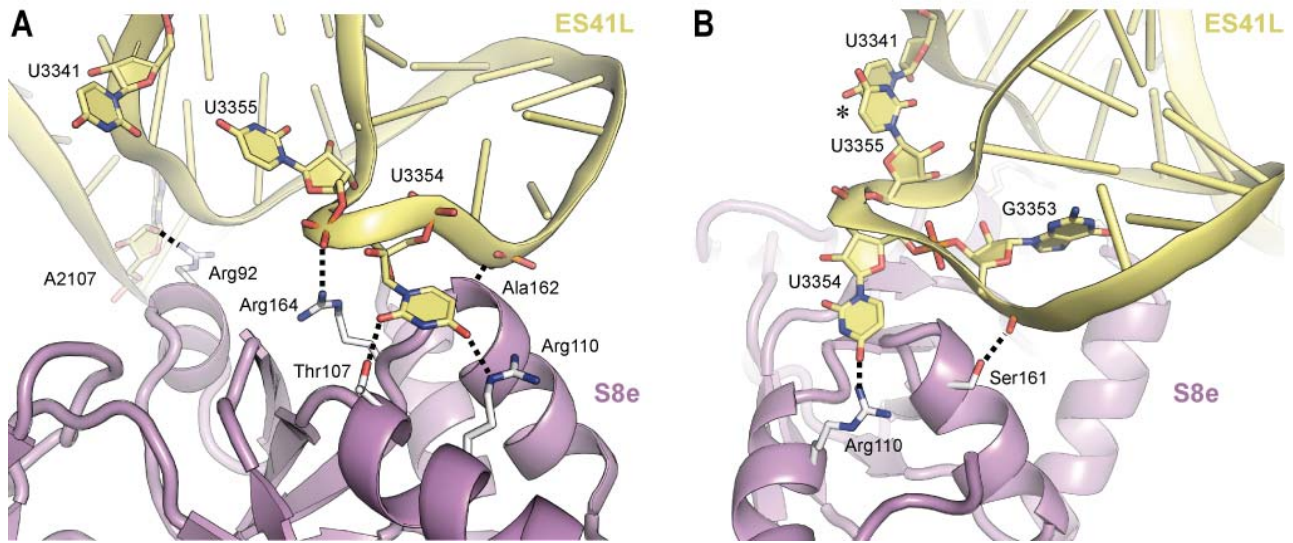


Fig. S13. Bridge eB1 is formed mainly by interactions between protein S8e and ES41L. **(A)** Bridge eB1 in ribosome A. **(B)** Rearrangement of the bridge in ribosome B. Compression of ES41L is important to maintain the bridge in ribosome B where the body of the small subunit rotates by an additional 5° compared to ribosome A. This compression is facilitated by stacking between two bases that occurs only in ribosome B (indicated by an asterisk).

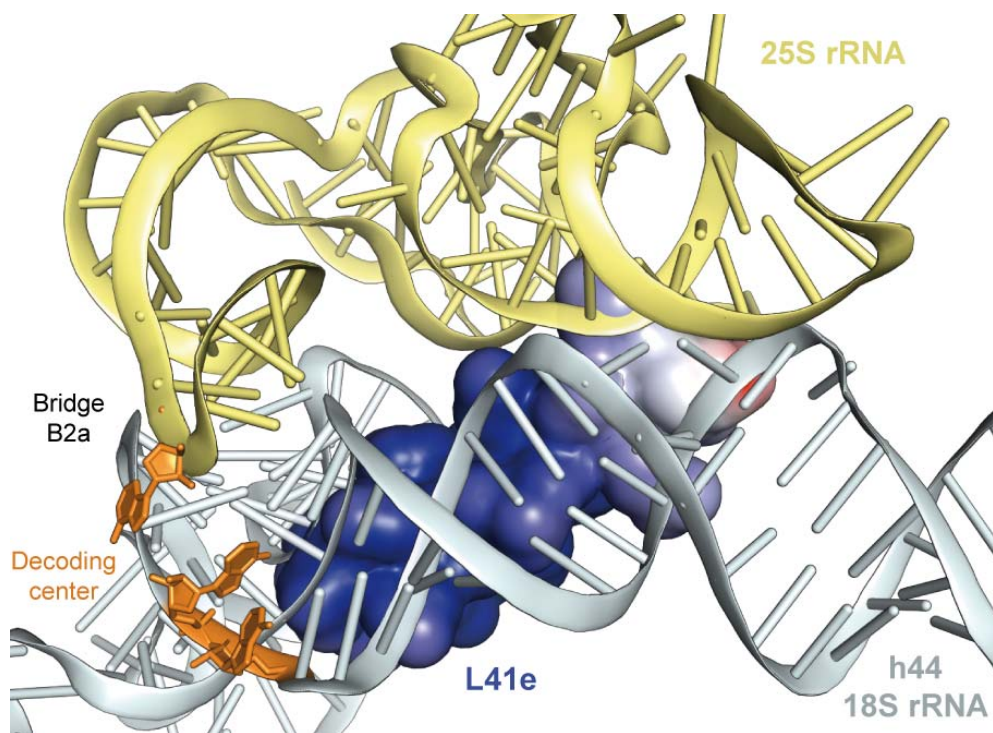


Fig. S14. Bridge eB14. Electrostatic potential surface representation of the highly positively charged L41e that extends from 60S into 40S in proximity of the decoding center.

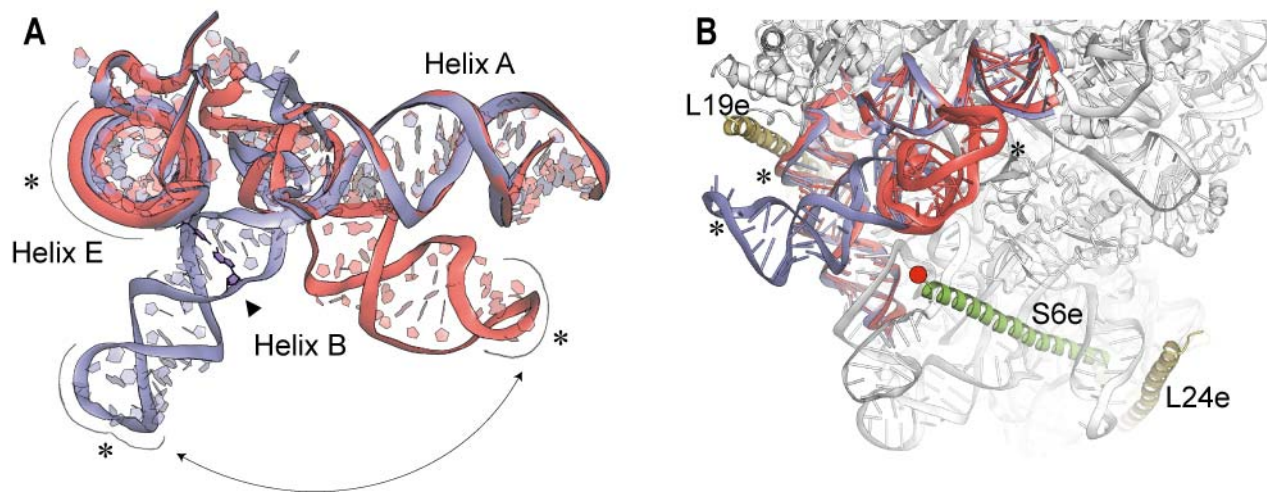


Fig. S15. Proximity of S6e C-terminal tail to the dynamic ES6S. **(A)** ES6S is a highly dynamic rRNA element of the small subunit that can adopt different conformations. ES6S is in red and blue in ribosome A and B, respectively. Black triangle indicates the location of a base-pair formed between ES6S helices B and E in ribosome B. **(B)** S6e C-terminus lies in proximity to ES6S. A red circle represents the last residue visible in our maps (10 additional residues could not be modeled). The two conformations of ES6S are shown and are colored as in A. Asterisks highlight ES6S residues in proximity of eIF4G binding site (29).

Table S1. Data collection, phasing and refinement statistics

Crystal and data collection statistics	
Space group	P2 ₁
Asymmetric unit	2 ribosomes (denoted as A and B) *
Unit cell dimensions (Å)	436.4300 * 288.2200 * 305.0800 $\beta = 98.99^\circ$
Resolution (Å)	301.0-3.0 (3.1-3.0) **
Redundancy - Bijvoet pairs merged - Bijvoet pairs not merged	38.4 (37.3) 19.4 (18.8)
Number of crystals merged	13
Completeness	100% (100%)
R _{meas} ***	31.7 (246.3)
R _{mrgd-F} ***	12.4 (66.2)
I/ σ (I)	14.8 (2.24)
SAD phasing statistics	
Heavy atom type	Osmium hexamine(III)
Wavelength (Å)	1.00
No. of sites	1360
Figure of Merit	0.35 (0.195)
Refinement statistics	
Resolution (Å)	301.0-2.9 (3.0-2.9) I/ σ (I) is 1.46, completeness is 100% for the highest resolution shell
Unique reflections	1639309
No. of Atoms	404714
R _{free} set	2.00%
R _{free} /R _{work} (%)	22.8/18.2
R.m.s. deviations :	
Bonds (Å)	0.013
Angles (°)	1.5

* Our earlier work at lower resolution described ribosome A at a similar unit cell (9).

** Numbers in parentheses refer to the highest resolution shell.

*** As defined in (56). The elevated R_{meas} is attributed to the high number of crystals and data-sets that were merged (13 crystals, these are never completely isomorphous) and to the method of data collection which results in a large number of relatively weak measurements of each reflection. The quality of individual measurements might be relatively low but the merged result has a higher signal to noise ratio due to averaging. R_{meas} compares individual measurements and does not take averaging into account whereas R_{mrgd-F} and I/ σ (I) do (56, 57).

Table S2. Summary of modeled ribosomal proteins and rRNA

Building summary - 60S subunit

Protein	Length	Built	Comment	Yeast name	Chain ID
L1	217	-		L1	
L2	254	2-253		L2	A
L3	387	2-387		L3	B
L4	362	2-362		L4	C
L18	297	2-297		L5	D
L6e	176	2-109; 129-176		L6	E
L30	244	23-244		L7	F
L8e	256	24-256		L8	G
L6	191	1-191		L9	H
L16	221	2-102; 111-221		L10	I
L5	174	6-174		L11	J
L11	165	9-155 ¹	Only in ribosome B	L12	K
L13e	199	2-194		L13	L
L14e	138	3-138		L14	M
L15e	204	2-204		L15	N
L13	199	3-199 ²		L16	O
L22	184	2-184	1-156 in ribosome B	L17	P
L18e	186	2-186		L18	Q
L19e	189	2-189		L19	R
L20e	172	1-172		L20	S
L21e	160	2-160		L21	T
L22e	121	11-108		L22	U
L14	137	2-137		L23	V
L24e	155	1-135	1-98 in ribosome A	L24	W
L23	142	22-142		L25	X
L24	127	2-127		L26	Y
L27e	136	2-136		L27	Z
L15	149	2-149		L28	a
L29e	59	2-58		L29	b
L30e	105	9-105		L30	c
L31e	113	4-112		L31	d
L32e	130	2-128		L32	e
L33e	107	2-107		L33	f
L34e	121	2-113		L34	g
L29	120	2-120		L35	h
L36e	100	2-100 ²		L36	i
L37e	88	2-88		L37	j
L38e	78	2-78		L38	k
L39e	51	2-51		L39	l
L40e	128 ³	77-128		L40	m
L41e	25	1-25		L41	n
L44e	106	2-106		L42	o
L43e	92	2-92		L43	p
P0	312	3-107; 182-221		P0	q
P1	106	1-46 ¹	Only in ribosome B	P1 α	r
P2	110	5-51 ¹	Only in ribosome B	P2 β	s

RNA	Length	Built
5S	121	1-121
5.8S	158	1-158
25S	3396	3-438; 492-1955; 2093-3396

Building summary – 40S subunit

Protein	Length	Built	Comment	Yeast name	Chain ID
S2	252	2-207		S0	A
S21e	255	20-233		S1	B
S5	254	34-250		S2	C
S3	240	3-225		S3	D
S4e	261	2-261		S4	E
S7	225	20-225		S5	F
S6e	236	1-226	1-218 in ribosome B	S6	G
S7e	190	4-187		S7	H
S8e	200	2-123; 135-200		S8	I
S4	197	2-186		S9	J
S10e	105	1-96		S10	K
S17	156	2-156		S11	L
S12e	143	20-143		S12	M
S15	151	2-151		S13	N
S11	137	11-137		S14	O
S19	142	7-131		S15	P
S9	143	4-143		S16	Q
S17e	136	2-89; 95-126		S17	R
S13	146	2-146		S18	S
S19e	144	2-144		S19	T
S10	121	15-121		S20	U
S21e	87	1-87		S21	V
S8	130	2-130		S22	W
S12	145	2-145		S23	X
S24e	135	2-135		S24	Y
S25e	108	37-105		S25	Z
S26e	119	2-98		S26	a
S27e	82	2-82		S27	b
S28e	67	5-67		S28	c
S14	56	5-56		S29	d
S30e	63	2-63		S30	e
S31e	152 ³	82-152		S31	f
RACK1	319	2-319		RACK1	g
Stm1	273	25-179		Stm1	h

RNA	Length	Built
18S	1800	1-665; 669-1799

¹ Modeled as poly-Ala

² The two yeast isoforms were modeled with occupancy of 50% for each.

³ Numbering is given according to the full-length gene product: S30e and L40e are expressed as fusions with ubiquitin which accounts for the first 76 amino acid residues. Ubiquitin moiety is not a part of the ribosomal proteins in mature ribosomes.

Table S3. Definition of expansion segments within 18S and 25S

40S subunit

rRNA ES	Coordinates
ES2	18S 125-142
ES3	18S 176-288
ES4B	18S 319-322
ES6A	18S 639-743
ES6B	18S 772-789
ES6C	18S 809-860
ES7	18S 1051-1067
ES9	18S 1353-1373
ES10	18S 1490-1493
ES12	18S 1682-1719

60S subunit

rRNA ES	Coordinates
ES4	25S 3-7; 5.8S 152-158
ES5	25S 115-160
ES6	25S 260-265
ES7	25S 437-622
ES8	25S 686-694
ES9	25S 714-786
ES10	25S 978-984
ES12	25S 1063-1101
ES13	25S 1190-1203
ES15	25S 1348-1356
ES19	25S 1554-1582
ES20	25S 1622-1653
ES26	25S 1804-1822
ES27	25S 1945-2103
ES31	25S 2521-2588
ES35	25S 2777-2785
ES39	25S 3152-3295
ES41	25S 3341-3362

* Definitions follow (58) but a small ES absent in (58) is named here ES4B

Table S4. Nomenclature of ribosomal proteins

To facilitate comparison between ribosomes from different species we adopted a nomenclature that is based on the names of protein families (www.uniprot.org/docs/ribosomp). This means that any core protein (i.e. with bacterial homologues) carries the bacterial name because this is the name given to the entire protein family. All proteins without homologues in bacteria have a name that ends with "e".

We applied in addition the following exceptions to that rule:

- P-stalk proteins retain their eukaryotic name in yeast (P0, P1, P2).
- The *S. cerevisiae* name (instead of the protein family name) is used for eukaryote-specific proteins whose protein family names are derived from mammals and have an additional "a" (59). Thus for example the yeast protein S1 which belongs to the protein family S3ae is called here S1e.

Small ribosomal subunit:

	Family name	Taxonomic range*	Bacteria name	Yeast name	Human name
1	S1e	A E	-	S1	S3A
2	S2	B A E	S2	S0	SA
3	S3	B A E	S3	S3	S3
4	S4	B A E	S4	S9	S9
5	S4e	A E	-	S4	S4
6	S5	B A E	S5	S2	S2
7	S6e	A E	-	S6	S6
8	S7	B A E	S7	S5	S5
9	S7e	E	-	S7	S7
10	S8	B A E	S8	S22	S15A
11	S8e	A E	-	S8	S8
12	S9	B A E	S9	S16	S16
13	S10	B A E	S10	S20	S20
14	S10e	E	-	S10	S10
15	S11	B A E	S11	S14	S14
16	S12	B A E	S12	S23	S23
17	S12e	E	-	S12	S12
18	S13	B A E	S13	S18	S18
19	S14	B A E	S14	S29	S29
20	S15	B A E	S15	S13	S13
21	S17	B A E	S17	S11	S11
22	S17e	A E	-	S17	S17
23	S19	B A E	S19	S15	S15
24	S19e	A E	-	S19	S19
25	S21e	E	-	S21	S21
26	S24e	A E	-	S24	S24
27	S25e	A E	-	S25	S25
28	S26e	E	-	S26	S26
29	S27e	A E	-	S27	S27
30	S28e	A E	-	S28	S28
31	S30e	A E	-	S30	S30
32	S31e	A E	-	S31	S27A
33	RACK1	E	-	Asc1	RACK1

* B – bacteria, A – archaea, E - eukaryotes

Large ribosomal subunit:

	Family name	Taxonomic range*	Bacteria name	Yeast name	Human name
1	L1	B A E	L1	L1	L10A
2	L2	B A E	L2	L2	L2
3	L3	B A E	L3	L3	L3
4	L4	B A E	L4	L4	L4
5	L5	B A E	L5	L11	L11
6	L6	B A E	L6	L9	L9
7	L6e	E	-	L6	L6
8	L8e	A E	-	L8	L7A
9	L11	B A E	L11	L12	L12
10	L13	B A E	L13	L16	L13A
11	L13e	A E [‡]	-	L13	L13
12	L14	B A E	L14	L23	L23
13	L14e	A E [‡]	-	L14	L14
14	L15	B A E	L15	L28	L27A
15	L15e	A E	-	L15	L15
16	L16	B A E	L16	L10	L10
17	L18	B A E	L18	L5	L5
18	L18e	A E	-	L18	L18
19	L19e	A E	-	L19	L19
20	L20e	E	-	L20	L18A
21	L21e	A E	-	L21	L21
22	L22	B A E	L22	L17	L17
23	L22e	E	-	L22	L22
24	L23	B A E	L23	L25	L23A
25	L24	B A E	L24	L26	L26
26	L24e	A E	-	L24	L24
27	L27e	E	-	L27	L27
28	L28e	E	-	-	L28
29	L29	B A E	L29	L35	L35
30	L29e	E	-	L29	L29
31	L30	B A E	L30	L7	L7
32	L30e	A E [‡]	-	L30	L30
33	L31e	A E	-	L31	L31
34	L32e	A E	-	L32	L32
35	L33e	A E [‡]	-	L33	L35A
36	L34e	A E [‡]	-	L34	L34
37	L36e	E	-	L36	L36
38	L37e	A E	-	L37	L37
39	L38e	A E [‡]	-	L38	L38
40	L39e	A E	-	L39	L39
41	L40e	A E [‡]	-	L40	L40
42	L41e	A E [‡]	-	L41	L41
43	L43e	A E	-	L43	L37A
44	L44e	A E	-	L42	L36A
45	P1 / P2	B A E	L12	P1/P2 (αβ)	LP1/LP2
46	P0	B A E	L10	P0	LPO

* B – bacteria, A – archaea, E – eukaryotes

‡ Proteins absent in the 50S structure from the archaea *H. marismortui* but occur in some (not all) archaeal organisms

Table S5. Components of intersubunit bridges in Ribosomes A and B

Ribosome A

		60S subunit		40S subunit	
Bridge	Component	Residue	Component	Residue	Comment
B1a	25S	1025 base	S19	Gln105 side chain	
	25S	1025 phosphate	18S	1239 phosphate	Mediated by Os
			18S	1240 phosphate	Mediated by Os
B1b/c	L5	Tyr116 side chain	S13	Arg110 side chain	Mediated by ion/water
	L5	Glu108 side chain	S13	Arg120 side chain	Mediated by ion/water
	L5	Glu80 side chain	S19	Arg108 side chain	Mediated by ion/water
	L5	Glu81 side chain	S19	Ala7 backbone	
	L5	Asp168 side chain	S19	Lys8 side chain	
	L5	Asp168 side chain	S19	Lys9 side chain	
	L5	Tyr89 side chain	S19	Val11 backbone	
B2a	25S	2257 base	18S	1646 backbone	
	25S	2258 base	18S	1646 backbone	
	25S	2259 base	18S	1645 backbone	
	25S	2255 base	18S	1644 backbone	
	25S	2262 base	18S	1644 backbone	OH-Pi hydrogen bond
	25S	2262 backbone	18S	1780 backbone+base	
	25S	2263 phosphate	18S	1780 base	
	25S	2263 phosphate	18S	1004 base	Mediated by Os
	25S	2264 phosphate			
	25S	2255 backbone	18S	1757 backbone	
	25S	2255 backbone	18S	1758 backbone	
	25S	2255 base	18S	1757 base	
	25S	2262 base	18S	1758 backbone+base	
	25S	2262 base	18S	1643 base	Mediated by ion/water
25S	2263 backbone	18S	1759 backbone		
B2b	25S	2272 phosphate	18S	996 phosphate	Mediated by hydrated Mg
	25S	2195 phosphate	18S	994 backbone	
	25S	2196 phosphate	18S	995 backbone	
	25S	2275 phosphate	18S	1779 phosphate	Mediated by Os
			18S	1780 phosphate	
B2c	25S	2151 phosphate	18S	984 phosphate	Mediated by Os
	25S	2191 phosphate	18S	982 phosphate	Mediated by Os
			18S	983 phosphate	
	25S	2192 phosphate	18S	981 phosphate	Mediated by Os
B3	25S	2290 base+backbone	18S	1746 backbone	
	25S	2291 backbone	18S	1746 backbone	
	25S	2291 backbone	18S	1655 base	
	25S	2303 backbone	18S	1747 backbone	
	25S	2302 base	18S	1746 base	Watson-crick-sugar edge base pair
	25S	2302 backbone	18S	1746 base	
	25S	2302 backbone	18S	1655 backbone	
	25S	2301 backbone	18S	1655 backbone	
	25S	2292 backbone	18S	1656 backbone	
	25S	2125 backbone	18S	1657 base	Stacking
	25S	2124 base	18S	1657 base	

	25S	1922 backbone	18S	1656 phosphate	Mediated by Os
	25S	2126 phosphate			
	25S	2305 phosphate	18S	1748 phosphate	Mediated by Os
			18S	1749 phosphate	
	25S	2294 phosphate	18S	1657 phosphate	Mediated by Os
			18S	1659 phosphate	
B4	25S	846 base	18S	971 base	
	25S	847 base	18S	972 backbone	
	25S	847 base	18S	973 backbone	
	25S	846 phosphate	18S	630 phosphate	Mediated by Mg
	25S	846 base	18S	628 backbone	Stacking
	25S	846 base	18S	972 base	
	25S	847 phosphate	S15	Lys140 side chain	
	L30e	Gly82 backbone	S15	Asn151 backbone	Mediated by hydrated Mg
B5	L14	Arg32 side chain	18S	1734 phosphate	
	L14	Asn28 side chain	18S	411 phosphate	
	L14	Thr115 side chain	18S	1734 phosphate	Mediated by hydrated Mg
	L14	Cys25 backbone			
	L14	Asp27 backbone			
	25S	1935 backbone	18S	1667 backbone	
B6	L24e	Arg43 side chain	18S	1670 phosphate	
	L24e	Arg47 side chain	18S	1724 backbone	
B7a	25S	2239 phosphate	18S	909 phosphate	Mediated by ion/water
	25S	2240 phosphate	18S	910 phosphate	Mediated by ion/water
	25S	2207 ?	18S	913 ?	Density is not clear
B7b/c	L2	Lys251 side chain	18S	987 phosphate	
			18S	986 phosphate	
	L2	Ser249 backbone	18S	987 base	
	L2	Gly248 backbone	18S	1013 phosphate	
	L2	Ser249 backbone	18S	1013 phosphate	
			18S	1012 phosphate	Mediated by ion/water
	L43e	Lys28 side chain	18S	983 backbone	
B8	L14	Ser133 backbone	18S	419 phosphate+base	Mediated by hydrated Mg
	L14	Gly134 backbone			
	L14	Ser112 side chain	18S	412 phosphate	
	L14	Asn28 side chain	18S	411 phosphate	
eB8	25S	2536 phosphate	S1e	Asp132 side chain	Mediated by ion/water
	25S	2537 phosphate	S1e	Asp 224 side chain	Mediated by ion/water
eB11	25S	3354 phosphate	S8e	Asp105 side chain	Mediated by ion/water
	25S	3354 base	S8e	Thr107 side chain	
	25S	3354 base	S8e	Arg110 side chain	
	25S	3355 phosphate	S8e	Arg164 side chain	
	25S	3353 phosphate	S8e	Ala162 backbone	
	25S	3345 phosphate	S8e	Arg92 side chain	
	25S	2107 backbone	S8e	Arg92 side chain	
eB12	L19e	Asn156 side chain	S17	Phe154	
	L19e	Glu160 side chain	S17	Phe156	
	L19e	Arg167 side chain	S17	Phe156	
	L19e	Arg162 side chain	18S	815 base	
	L19e	Arg163 side chain	18S	813 base	
	L19e	Lys165 side chain	18S	850 phosphate	
			18S	851 phosphate	
	L19e	Asn166 side chain	18S	815 phosphate	
	L19e	Arg170 side chain	18S	814 phosphate	
			18S	815 phosphate	
	L19e	Arg172 side chain	18S	851 phosphate	
			18S	852 phosphate	
	L19e	Arg173 side chain	18S	855 base	
	L19e	Arg176 side chain	18S	852 phosphate	
			18S	853 phosphate	
	L19e	Lys180 side chain	18S	854 phosphate	
eB13	L3	Ser297 backbone	S6e	His22 side chain	Mediated by ion/water

	L3	Phe298 backbone	S6e	Arg25 side chain	Mediated by ion/water
	L3	Arg300 side chain	S6e	His22 side chain	
	L24e	Pro81 side chain	S6e	Pro130 side chain	
	L24e	Ile82 side chain	S6e	Phe144 side chain	
	L24e	Thr83 side chain	S6e	Arg132 backbone	
	L24e	Gly84 backbone	S6e	Arg159 backbone	
	L24e	Ile90 side chain	S6e	Phe144 side chain	
	L24e	Arg93 side chain	S6e	Phe145 side chain	
	L24e	Arg93 side chain	S6e	Phe156 side chain	
	L24e	Arg94 side chain	S6e	Phe144 backbone	
eB14	L41e	Met1 backbone	18S	1641 phosphate	
	L41e	Arg2 backbone	18S	1783 phosphate	
	L41e	Arg2 side chain	18S	1773 phosphate	
	L41e	Lys4 backbone	18S	1773 phosphate	
	L41e	Lys4 side chain	18S	1774 base	
	L41e	Trp5 side chain	18S	1783 base	
			18S	1784 base	
			18S	1785 base	
	L41e	Arg6 side chain	18S	1112 phosphate	
	L41e	Lys7 side chain	18S	1774 phosphate	
	L41e	Lys8 side chain	18S	1777 base	
			18S	1778 base	
	L41e	Arg9 side chain	18S	1782 phosphate	
	L41e	Arg9 side chain	18S	1642 backbone	
	L41e	Thr10 side chain	18S	1114 phosphate	Mediated by ion/water
	L41e	Arg11 side chain	18S	1775 phosphate	
			18S	1127 phosphate	
	L41e	Arg12 side chain	18S	1779 base	
			18S	1778 base	
	L41e	Lys14 side chain	18S	1115 phosphate	
	L41e	Arg15 side chain	18S	1126 phosphate	
	L41e	Arg17 side chain	18S	1116 phosphate	
	L41e	Arg18 side chain	18S	1126 phosphate	
			18S	1125 phosphate	
	L41e	Arg21 side chain	18S	1654 phosphate	
			18S	1118 phosphate	
			18S	1117 phosphate	
	L41e	Ser24 side chain	18S	1655 phosphate	

Ribosome B

60S subunit			40S subunit		
Bridge	Component	Residue	Component	Residue	Comment
B1a	-	-	-	-	Broken interactions
B1b/c	L5	Tyr116 side chain	S13	Arg 110 side chain	
			S13	Asp111 side chain	Mediated by ion/water
	L5	Glu108 side chain	S13	Lys118 side chain	
	L5	Lys85 side chain	S19	Phe42 side chain	
	L5	Glu88 side chain	S19	Arg10 side chain	
	L5	Glu90 side chain	S19		
	L5	Asp168 side chain	S19	Lys 9 side chain	
	L5	Gln90 side chain	S19	Asn70 side chain	
B2a	25S	2257 base	18S	1646 backbone	
	25S	2258 base	18S	1646 backbone	
	25S	2259 base	18S	1645 backbone	
	25S	2255 base	18S	1644 backbone	
	25S	2262 base	18S	1644 backbone	OH-Pi hydrogen bond
	25S	2262 backbone	18S	1780 backbone+base	
	25S	2263 phosphate	18S	1780 base	
	25S	2263 phosphate	18S	1004 base	Mediated by Os
	25S	2264 phosphate			
	25S	2255 backbone	18S	1757 backbone	
	25S	2255 backbone	18S	1758 backbone	
	25S	2255 base	18S	1757 base	
	25S	2262 base	18S	1758 backbone+base	
	25S	2262 base	18S	1643 base	Mediated by water
	25S	2263 backbone	18S	1759 backbone	
B2b	25S	2275 phosphate	18S	1780 phosphate	
			18S	1781 phosphate	
	25S	2197 phosphate	18S	996 phosphate	Mediated by hydrated Mg
	25S	2196 phosphate			
	25S	2274 phosphate	18S	1779 phosphate	Mediated by hydrated Mg
B2c	25S	2191 phosphate	18S	982 phosphate	Mediated by Os
			18S	983 phosphate	
B3	25S	2290 base+backbone	18S	1746 backbone	
	25S	2291 backbone	18S	1746 backbone	
	25S	2291 backbone	18S	1655 base	
	25S	2303 backbone	18S	1747 backbone	
	25S	2302 base	18S	1746 base	Watson-crick-sugar edge base pair
	25S	2302 backbone	18S	1746 base	
	25S	2302 backbone	18S	1655 backbone	
	25S	2301 backbone	18S	1655 backbone	
	25S	2292 backbone	18S	1656 backbone	
	25S	2125 backbone	18S	1657 base	Stacking
	25S	2124 base	18S	1657 base	
	25S	1922 backbone	18S	1656 phosphate	Mediated by Os
	25S	2126 phosphate			
	25S	2305 phosphate	18S	1748 phosphate	Mediated by Os
			18S	1749 phosphate	
	25S	2303 phosphate	18S	1747 base+backbone	Mediated by hydrated Mg
	25S	2294 phosphate	18S	1657 phosphate	Mediated by Os
				1659 phosphate	
B4	25S	847 base	18S	973 backbone	
	25S	848 base	18S	973 backbone	
	25S	847 base	18S	972 backbone	
	25S	848 base	18S	972 backbone	
	25S	846 base	18S	972 backbone	

	25S	846 base	18S	972 backbone	
	25S	846 base	18S	628 backbone	Stacking
	25S	847 phosphate	S15	Tyr141 backbone	Mediated by ion/water
	25S	847 phosphate	S15	Lys140 backbone	Mediated by ion/water
	25S	846 backbone	S15	His123 sidechain	Stacking
	25S	845 base	S15	Glu142 sidechain	Mediated by Os
	25S	844 phosphate			
B5	L14	Arg32 side chain	18S	1734 phosphate	
	L14	Asn28 side chain	18S	411 phosphate	
	L14	Thr115 side chain	18S	1734 phosphate	Mediated by Os
	L14	Cys25 backbone			
	L14	Asp27 backbone			
	25S	1935 backbone	18S	1667 backbone	
	25S	1936 phosphate	18S	1667 backbone	
B6	L24e	Arg43 side chain	18S	1670 phosphate	
	L24e	Arg47 side chain	18S	1724 backbone	
B7a	25S	2205 base	18S	913 base	Stacking
	25S	2205 base	18S	911 phosphate	
B7b/c	L2	Tyr133 side chain	18S	986 phosphate	Mediated by ion/water
	L2	Gln250 side chain	18S	988 phosphate	
	L2	Arg147 side chain	18S	892 backbone	
	L43e	Gln25 side chain	18S	983 backbone	
	L43e	Arg85 side chain	18S	923 phosphate	
	L43e	Lys6 side chain	18S	1122 phosphate	
	L2	Asp176 side chain	18S	984 backbone	
	L43e	Arg24 side chain	18S	982 backbone	
L43e	Ala74 side chain	18S	985 backbone		
B8	L14	Ser133 backbone	18S	419 base	Mediated by Os
	L14	Gly134 backbone			
	L14	Ser131 backbone			
	L14	Ser112 side chain	18S	412 phosphate	
	L14	Asn28 side chain	18S	411 phosphate	
eB8	L43e	Ala92 backbone	S1e	Lys219 side chain	
	L43e	Ala92 backbone	S1e	Lys128 side chain	
	18S	A2535 backbone	S1e	Asp224 side chain	
	18S	U2533 phosphate	S1e	Asp234 side chain	Mediated by ion/water
eB11	18S	U3354 base	S8e	Thr107 side chain	
	18S	U3354 base	S8e	Arg110 side chain	
	18S	U3353 phosphate	S8e	Ser161 backbone	
	18S	G3345 phosphate	S8e	Arg92 side chain	Mediated by ion/water
	18S	U3346 phosphate	S8e	Lys199 side chain	
eB12	L19e	Arg162 side chain	18S	815 base	
	L19e	Arg163 side chain	18S	813 base	
	L19e	Lys165 side chain	18S	850 phosphate	
			18S	851 phosphate	
	L19e	Asn166 side chain	18S	815 phosphate	
	L19e	Arg167 side chain	18S	814 phosphate	
	L19e	Arg170 side chain	18S	814 phosphate	
			18S	815 phosphate	
	L19e	Arg172 side chain	18S	851 phosphate	
			18S	852 phosphate	
	L19e	Arg173 side chain	18S	855 base	
	L19e	Arg176 side chain	18S	852 phosphate	
			18S	853 phosphate	
	L19e	Lys180 side chain	18S	854 phosphate	
L19e	Leu185 backbone	S7e	Arg39 side chain		
L19e	Ala189 backbone	S7e	Ser2 side chain		
eB13	L3	Ser297 backbone	S6e	His22 side chain	Mediated by ion/water
	L3	Phe298 backbone	S6e	Arg25 side chain	Mediated by ion/water
	L24e	Lys70 side chain	18S	1714 phosphate	
	L24e	Arg71 side chain	18S	1713 phosphate	
	L24e	Arg73 side chain	18S	1712 phosphate	

	L24e	Pro81 side chain	S6e	Pro130 side chain		
	L24e	Ile82 side chain	S6e	Phe144 side chain		
	L24e	Thr83 side chain	S6e	Arg132 backbone		
	L24e	Gly84 backbone	S6e	Arg159 backbone		
	L24e	Ile90 side chain	S6e	Phe144 side chain		
	L24e	Arg93 side chain	S6e	Phe145 side chain		
	L24e	Arg93 side chain	S6e	Phe156 side chain		
	L24e	Arg94 side chain	S6e	Phe144 backbone		
	L24e	Arg101 side chain	S6e	Asp151 side chain		
	L24e	Arg105 side chain	S6e	Glu150 side chain		
	L24e	Lys108 side chain	S6e	Asp155 side chain		
	L24e	Asp112 side chain	18S	280 base		
	L24e	Lys113 side chain	18S	280 phosphate		
	L24e	Lys117 side chain	18S	278 base		
	L24e	Asp119 side chain	18S	75 base		
	L24e	Lys120 side chain	18S	274 phosphate		
	L24e	Arg123 side chain	18S	273 phosphate		
	L24e	Lys124 side chain	18S	274 phosphate		
eB14	L41e	Met1 backbone	18S	1641 phosphate		
	L41e	Arg2 backbone	18S	1783 phosphate		
	L41e	Arg2 side chain	18S	1773 phosphate		
	L41e	Lys4 backbone	18S	1773 phosphate		
	L41e	Lys4 side chain	18S	1774 base		
	L41e	Trp5 side chain	18S	1783 base		
				18S	1784 base	
				18S	1785 base	
	L41e	Arg6 side chain	18S	1112 phosphate		
	L41e	Lys7 side chain	18S	1774 phosphate		
	L41e	Lys8 side chain	18S	1777 base		
				18S	1778 base	
	L41e	Arg9 side chain	18S	1782 phosphate		
	L41e	Arg9 side chain	18S	1642 backbone		
	L41e	Thr10 side chain	18S	1114 phosphate	Mediated by ion/water	
	L41e	Arg11 side chain	18S	1775 phosphate		
				18S	1127 phosphate	
	L41e	Arg12 side chain	18S	1779 base		
				18S	1778 base	
	L41e	Lys14 side chain	18S	1115 phosphate		
	L41e	Arg15 side chain	18S	1126 phosphate		
	L41e	Lys16 side chain	18S	1750 phosphate		
	L41e	Arg17 side chain	18S	1116 phosphate		
	L41e	Arg18 side chain	18S	1126 phosphate		
				18S	1125 phosphate	
	L41e	Arg21 side chain	18S	1654 phosphate		
				18S	1118 phosphate	
				18S	1117 phosphate	
	L41e	Ser24 side chain	18S	1655 phosphate		

Additional References

39. M. P. Ashe, S. K. De Long, A. B. Sachs, *Mol. Biol. Cell* **11**, 833 (2000).
40. B. Lang *et al.*, *Anal. Biochem.* **77**, 110 (1977).
41. G. Huelsen, C. Broennimann, E. F. Eikenberry, A. Wagner, *J. Appl. Crystallogr.* **39**, 550 (2006).
42. W. Kabsch, *Acta Crystallogr. D* **66**, 125 (2010).
43. Collaborative Computational Project 4, *Acta Crystallogr. D* **50**, 760 (1994).
44. P. D. Adams *et al.*, *Acta Crystallogr. D* **66**, 213 (2010).
45. A. J. McCoy *et al.*, *J. Appl. Crystallogr.* **40**, 658 (2007).
46. K. Cowtan, *Acta Crystallogr. D* **66**, 470 (2010).
47. J. P. Abrahams, A. G. Leslie, *Acta Crystallogr. D* **52**, 30 (1996).
48. A. T. Brünger *et al.*, *Acta Crystallogr. D* **54**, 905 (1998).
49. P. Emsley, K. Cowtan, *Acta Crystallogr. D* **60**, 2126 (2004).
50. N. A. Baker, D. Sept, S. Joseph, M. J. Holst, J. A. McCammon, *Proc. Natl. Acad. Sci. U.S.A.* **98**, 10037 (2001).
51. W. Humphrey, A. Dalke, K. Schulten, *J. Mol. Graphics* **14**, 33 (1996).
52. Y. Ye, A. Godzik, *Bioinformatics* **19** (suppl. 2), ii246 (2003).
53. W. L. DeLano, The PyMOL Molecular Graphics System, Version 1.4, Schrödinger LLC. www.pymol.org.
54. R. Beckmann *et al.*, *Cell* **107**, 361 (2001).
55. J. P. Armache *et al.*, *Proc. Natl. Acad. Sci. U.S.A.* **107**, 19748 (2010).
56. K. Diederichs, P. A. Karplus, *Nat. Struct. Biol.* **4**, 269 (1997).
57. Q. Liu, Z. Zhang, W. A. Hendrickson, *Acta Crystallogr. D* **67**, 45 (2011).
58. S. A. Gerbi, *Biosystems* **19**, 247 (1986).
59. W. H. Mager *et al.*, *Nucleic Acids Res.* **25**, 4872 (1997).